Ice nucleating particles at a coastal marine boundary layer site: correlations with aerosol type and meteorological conditions

Authors: R. H. Mason[1], M. Si[1], J. Li[2], C. Chou[1], R. Dickie[1], D. Toom-Sauntry[3], C. Pöhlker[4], J. D. Yakobi-Hancock[5], L. A. Ladino[5], K. Jones[6], W. R. Leaitch[3], C. L. Schiller[6], J. P. D. Abbatt[5], J. A. Huffman[2*], A. K. Bertram[1*]

Affiliations:

[1]Department of Chemistry, University of British Columbia, Vancouver, BC, V6T1Z1, Canada

[2]Department of Chemistry and Biochemistry, University of Denver, Denver, CO, 80208, USA

[3]Climate Research Division, Environment Canada, Toronto, ON, M3H5T4, Canada

[4]Biogeochemistry Department, Max Planck Institute of Chemistry, Mainz, 55020, Germany

[5]Department of Chemistry, University of Toronto, Toronto, ON, M5S3H6, Canada

[6]Air Quality Science Unit, Environment Canada, Vancouver, BC, V6C3S5, Canada

[*]Correspondence to: bertram@chem.ubc.ca (A. K. Bertram), alex.huffman@du.edu (J. A. Huffman)

Abstract:

Information on what aerosol particle types are the major sources of ice nucleating particles (INPs) in the atmosphere is needed for climate predictions. To determine which aerosol particles are the major sources of immersion-mode INPs at a coastal site in Western Canada, we investigated correlations between INP number concentrations and both concentrations of different atmospheric particles and meteorological conditions. We show that INP number concentrations are strongly correlated with the number concentrations of fluorescent bioparticles between -15 and -25 °C, and that the size distribution of INPs is most consistent with the size distribution of fluorescent bioparticles. We conclude that biological particles were likely the major source of ice nuclei at freezing temperatures between -15 and -25 °C at this site for the time period studied. At -30 °C, INP number concentrations are also well correlated with number concentrations of the total aerosol particles ≥ 0.5 μm, suggesting that non-biological particles may have an important contribution to the population of INPs active at this temperature. As we found that black carbon particles were unlikely to be a major source of ice nuclei during this study, these non-biological INPs may include mineral dust. Furthermore, correlations involving chemical tracers of marine aerosols and marine biological activity, sodium and methanesulfonic acid, indicate that the majority of INPs measured at the coastal site likely originated from terrestrial rather than marine sources. Finally, six existing empirical parameterizations of ice nucleation were tested to determine if they accurately predict the measured INP number concentrations. We found that none of the parameterizations selected are capable of predicting INP number concentrations with high accuracy over the entire temperature range investigated. This finding illustrates that additional measurements are needed to improve parameterizations of INPs and their subsequent climatic impacts.

1. Introduction

The formation of ice in the atmosphere can occur by two primary mechanisms: homogeneous and heterogeneous ice nucleation. Homogeneous nucleation can only occur at temperatures below approximately -37 °C. However, heterogeneous nucleation can occur at all temperatures below 0 °C. In the atmosphere, heterogeneous nucleation occurs on solid or partially solid aerosol particles termed ice nucleating particles (INPs). INPs are a small subset of the total aerosol population (Rogers et al., 1998) whose unique surface properties make them capable of lowering the energy barrier to ice nucleation and hence cause freezing at warmer temperatures or lower supersaturations with respect to ice compared to homogeneous nucleation. Four modes of nucleation have been identified (Vali, 1985; Vali et al., 2015): deposition nucleation where ice forms on the INP directly from the gas phase; condensation freezing where ice forms during the condensation of water onto the INP; immersion freezing where ice forms on an INP within a supercooled droplet; and contact freezing where the impact of a supercooled droplet by an INP initiates freezing. In this study we focus on immersion freezing, which is relevant to ice formation in mixed-phase clouds.

The presence of INPs in the atmosphere can lead to changes in the microphysical properties and lifetime of clouds. As a result, a change in INP concentrations can indirectly modify climate by changing cloud optical properties, lifetime, and cloud extent (e.g. Baker, 1997; Lohmann, 2002; Storelvmo et al., 2011; Creamean et al., 2013). Currently, the role of INPs in climate change is highly uncertain (Boucher et al., 2013). To predict the role of INPs in climate change and precipitation, information on what particle types are the major sources of INPs in the atmosphere is needed. Possible candidates for INPs in the atmosphere include mineral dust, primary biological particles, and black carbon (BC). Primary biological INPs are

74 believed to be dominant above -15 °C while below this temperature non-biological INPs may be
75 of greater importance (Murray et al., 2012).

76 Mineral dust particles have long been known to be efficient INPs (Mason and Maybank,
77 1958). Numerous laboratory studies have found that different types of mineral dust particles can
78 effectively nucleate ice in both the immersion and deposition modes; for example kaolinite
79 (Lüönd et al., 2010; Wheeler and Bertram, 2012), Arizona test dust (Kanji and Abbatt, 2010;
80 Knopf and Koop, 2006; Marcolli et al., 2007; Niedermeier et al., 2010), NX illite (Broadley et
81 al., 2012), natural Asian and Saharan dust samples (Field et al., 2006; Kulkarni, 2010), and more
82 recently feldspar (Atkinson et al., 2013; Yakobi-Hancock et al., 2013). Both field studies
83 (DeMott et al., 2003; Cziczo et al., 2004; Richardson et al., 2007; Klein et al., 2010; Chou et al.,
84 2011; Creamean et al., 2013) and modeling studies (Hoose et al., 2010b) also suggest that
85 mineral dust can be a dominant INP in the atmosphere.

86 Primary biological particles have also been identified as a possible source of INPs (e.g.
87 Szyrmer and Zawadzki, 1997; Möhler et al., 2007; Garcia et al., 2012; Hiranuma et al., 2015).
88 The ocean and continents are both potential sources of ice-active primary biological particles
89 (Hoose and Möhler, 2012; Murray et al., 2012). Model studies have shown that biological
90 particles may not be important for ice nucleation on a global and annual scale (Hoose et al.,
91 2010a; Sesartic et al., 2013; Spracklen and Heald, 2014), but may be important on regional and
92 seasonal scales, especially if concentrations of biological particles are high or concentrations of
93 other types of INPs are low (Phillips et al., 2009; Sun et al., 2012; Burrows et al., 2013;
94 Creamean et al., 2013; Yun and Penner, 2013; Costa et al., 2014; Spracklen and Heald, 2014).

95 Ice-active biological particles from continental sources include bacteria (e.g. Maki et al.,
96 1974; Lindow et al., 1978; Maki and Willoughby, 1978; Kozloff et al., 1983), fungal spores (e.g.

97 Jayaweera and Flanagan, 1982; Tsumuki et al., 1992; Richard et al., 1996; Iannone et al., 2011;
98 Haga et al., 2013; Morris et al., 2013), and pollen (e.g. Diehl et al., 2001, 2002; von Blohn et al.,
99 2005; Pummer et al., 2012; Augustin et al., 2013; Hader et al., 2014; O'Sullivan et al., 2015). In
100 addition, strong correlations between number concentrations of INPs and primary biological
101 particles have been found during studies in the Amazon and United States in forested regions
102 (Prenni et al., 2009, 2013; Huffman et al., 2013; Tobo et al., 2013). Ice-active biological particles
103 have also been observed at high concentrations above a corn field during combine harvesting
104 (Garcia et al., 2012). Biological particles have been observed in ice-crystal residuals of mixed-
105 phase clouds (e.g. Pratt et al., 2009), cloud water (e.g. Joly et al., 2014), and snow samples (e.g.
106 Christner et al., 2008; Morris et al., 2008; Hill et al., 2014), and ice-active biological particles
107 have also been associated with soils (Conen et al., 2011; O'Sullivan et al., 2014; Tobo et al.,
108 2014; Fröhlich-Nowoisky et al., 2015).

109 Biological material found in the ocean that may be a source of INP in the atmosphere
110 include phytoplankton, bacteria, and biological material in the sea surface microlayer. Studies
111 have indicated bacteria and phytoplankton found in seawater and sea ice are a potential source of
112 INP in the atmosphere (Schnell, 1975, 1977; Schnell and Vali, 1975; Jayaweera and Flanagan,
113 1982; Parker et al., 1985; Alpert et al., 2011; Knopf et al., 2011). Material in the sea surface
114 microlayer has also been found to exhibit ice-activity (Wilson et al., 2015), and previous work
115 has indicated that biological material generated during phytoplankton blooms may be a source of
116 INPs in the atmosphere (Prather et al., 2013; DeMott et al., 2015). The modeling work of
117 Burrows et al. (2013) indicates that ice-active primary biological particles from the ocean may be
118 particularly important in remote regions such as the Southern Ocean.

119 Another potential type of INP in the atmosphere is BC particles (Kärcher et al., 2007).

Field studies have produced varying results on the relative importance of these particles as a source of ice nuclei in the atmosphere (e.g. Lin et al., 2006; Cozic et al., 2008; Kamphus et al., 2010; Twohy et al., 2010; Ebert et al., 2011; Corbin et al., 2012; Cziczo et al., 2013; Knopf et al., 2014; McCluskey et al., 2014). Laboratory studies suggest that the ability of BC particles to act as INPs may depend strongly on the method of generating these particles, including the fuel type (e.g. Diehl and Mitra, 1998; Gorbunov et al., 2001; Möhler et al., 2005; Dymarska et al., 2006; Kärcher et al., 2007; DeMott et al., 2009; Petters et al., 2009; Friedman et al., 2011; Cziczo et al., 2013; Brooks et al., 2014). For example, the combustion of some biomass burning fuels emits more efficient INPs when compared to combustion of some fossil fuels (e.g. Petters et al., 2009; McCluskey et al., 2014). BC is generally considered to be less efficient than mineral dust in the immersion mode (Hoose and Möhler, 2012; Murray et al., 2012; and references therein). Models have suggested that carbonaceous aerosols may have a significant indirect effect on climate if they efficiently nucleate ice (e.g. Lohmann, 2002; Liu et al., 2009; Penner et al., 2009; Yun and Penner, 2013).

To determine which aerosol particles are the major source of INPs in the immersion mode at a coastal site in Western Canada, we investigate correlations between INP number concentrations and both concentrations of different atmospheric particle types and meteorological conditions. Measurements were conducted in August 2013 as part of the NETwork on Climate and Aerosols: addressing key uncertainties in Remote Canadian Environments (NETCARE) project (http://netcare-project.ca/). A primary goal of the study was to investigate whether primary biological particles and black carbon (BC) particles are a major source of INPs at this site and determine if the ocean contributes to the measured INP population at this coastal site. In addition, we also test the ability of parameterizations reported in the

143 literature at predicting the INP number concentrations measured at this coastal site.

144 **2. Methods**

145 **2.1 Site description and instrument location**

146 Measurements were performed at Amphitrite Point (48.92° N, 125.54° W) on the west
147 coast of Vancouver Island in British Columbia, Canada. This was also the location of studies on
148 ozone (McKendry et al., 2014) and cloud condensation nuclei (Yakobi-Hancock et al., 2014).
149 Amphitrite Point (Fig. 1) is located approximately 2.2 km south of the town of Ucluelet
150 (population of 1627 in 2011; Statistics Canada, 2012). The largest nearby population centers are
151 Nanaimo 120 km to the east, Victoria 170 km to the southeast, and Vancouver 180 km to the
152 east. This region has a temperate maritime climate, characterized by warm summers, mild
153 winters, and relatively high levels of cloud cover and precipitation. According to the Köppen-
154 Geiger classification scheme (Kottek et al., 2006), the climate type is Cfb which denotes a mild
155 mid-latitude and moist climate (C) with no dry season (f), and a moderate summer where the
156 average hottest-month temperature is < 22 ºC and at least four months have an average
157 temperature > 10 ºC (b). Local forests contain predominantly coniferous tree species including
158 western hemlock, western redcedar, and Douglas-fir that is characteristic of most low-elevation
159 sites along the west coast of Canada (Austin et al., 2008). The Pacific Ocean is west and south of
160 the site, where the mixing of iron-rich coastal waters with nitrate-rich oceanic waters produces a
161 zone of high primary productivity (Whitney et al., 2005; Ribalet et al., 2010). Measurements
162 were carried out from August 6–27, 2013. Specifics on the sampling times (i.e. start and end
163 times) are given in Table S1 of the Supplement.

164 Aerosol instrumentation was located in one of two mobile laboratories; one specific to
165 the NETCARE project (labeled 1 in Fig. 1) and one operated by Environment Canada, the

166 British Columbia Ministry of Environment, and Metro Vancouver (labeled 2 in Fig. 1). Aerosols
167 were sampled through louvered total suspended particulate inlets (Mesa Labs Inc., Butler, NJ,
168 USA) or louvered PM_{10} inlets (Thermo Scientific, Waltham, MA, USA) atop masts extending
169 5.5 m agl. The two mobile laboratories were approximately 20 m above mean sea level and 100
170 m from the high tide line of the Pacific Ocean (McKendry et al., 2014). A row of trees and
171 shrubs approximately 2–10 m in height stood between the laboratories and the rocky shoreline.
172 Adjacent to the laboratories on their seaward side was Amphitrite Lighthouse (labeled 3 in Fig.
173 1) and Wild Pacific Trail, local tourist attractions and a source of foot traffic during fair weather.
174 Immediately north and east of the site was a station of the Canadian Coast Guard (labeled 4 in
175 Fig. 1).

176 The majority of the meteorological parameters reported in this study were measured at
177 Amphitrite Lighthouse, located approximately halfway between the mobile laboratories and the
178 ocean. Relative humidity and temperature were monitored using an HMP45C probe (Campbell
179 Scientific, Logan, UT, USA) with accuracies of ± 3 % and ± 0.2 °C, respectively. Wind direction
180 and wind speed were determined by a model 05305L Wind Monitor (R. M. Young, Traverse
181 City, Michigan, USA) to a respective accuracy of ± 3° and ± 0.2 m s^{-1}. Measurements of wind
182 speed were also obtained from a moored buoy located in La Perouse Bank, approximately 35 km
183 to the WSW of the Amphitrite Point sampling site (station 46206; 48.84° N, 126.00 °W;
184 National Data Buoy Center, 2013). The cup anemometer used to measure wind speed on the
185 buoy was positioned at 5 m asl.

186 **2.2 Ice nucleating particle measurements**

187 INP number concentrations in the immersion mode were determined using the micro-
188 orifice uniform deposit impactor-droplet freezing technique (MOUDI-DFT; Mason et al., 2015).

A Model II 120R MOUDI (MSP Corp., Shoreview, MN, USA) collected size-fractionated aerosol samples by inertial separation (Marple et al., 1991) onto hydrophobic glass cover slips (HR3-215; Hampton Research, Aliso Viejo, CA, USA). To compensate for the thickness of the hydrophobic glass cover slips, spacers were placed between the MOUDI stages. Custom substrate holders were added to the MOUDI impaction plates to maintain consistent positioning of the hydrophobic glass cover slips within the impactor (Mason et al., 2015). Samples from MOUDI stages 2–8 were used in this study, corresponding to a particle size range of 10–0.18 μm (50 % cutoff aerodynamic diameter). Thirty-four sets of MOUDI samples were collected; 18 during the day and 16 at night. The average collection time of a MOUDI sample was 7.8 hours. Details of each INP sampling period are available in Table S1 of the Supplement.

The ice-nucleating ability of particles collected by the MOUDI was then determined by the droplet freezing technique (DFT; Koop et al., 2000; Iannone et al., 2011; Mason et al., 2015; Wheeler et al., 2015). Within 24 hours of collection, samples were placed in a temperature- and humidity-controlled flow cell that was coupled to an optical microscope (Axiolab; Zeiss, Oberkochen, Germany) with a 5× magnification objective. At a sample temperature of 0 °C a humidified gas flow was introduced, resulting in the formation of water droplets on the sample. Following droplet growth by condensation and coalescence, the droplet size was decreased with a dry gas flow to a final size of approximately 80–160 μm in diameter. On average, more than 99 % of particles on the surface of the hydrophobic glass cover slip were incorporated into droplets by this procedure. Closing valves upstream and downstream of the cell then isolated the flow cell, and the sample temperature was lowered at a constant rate of -10 °C min^{-1} to -40 °C. This cooling rate was chosen to minimize the freezing of a liquid droplet by contact with a growing ice crystal. Recent work suggests that changing the cooling rate by an order of magnitude may

lead to a shift in freezing temperatures of approximately 0.5–2 °C (Murray et al., 2011; Broadley et al., 2012; Welti et al., 2012; Wright and Petters, 2013; Wright et al., 2013; Wheeler et al., 2015). During droplet growth, evaporation, and cooling, a CCD camera connected to the optical microscope recorded a digital video of the sample. Using the video timestamp and a resistance temperature detector positioned within the flow cell, which was calibrated against the melting point of water droplets approximately 100 μm in diameter, the freezing temperature of each droplet was found by manually noting the increase in droplet opacity immediately following ice nucleation.

Since a small fraction of the sampled particles (less than 1 % on average) was not included in the droplets, there was the possibility of deposition nucleation as well. However, based on an analysis of the videos recorded during the ice nucleation experiments, fewer than 3 % of all freezing events observed were the result of deposition nucleation. Due to the low occurrence of deposition nucleation, only immersion freezing results are reported.

The atmospheric number concentration of INPs within the size cut of each MOUDI stage, [INPs(T)], was evaluated using the following equation:

$$[\mathrm{INPs}(T)] = -\ln\left(\frac{N_\mathrm{u}(T)}{N_\mathrm{o}}\right) N_\mathrm{o} \left(\frac{A_\mathrm{deposit}}{A_\mathrm{DFT} V}\right) f_\mathrm{nu} f_\mathrm{ne} \qquad (1)$$

where $N_\mathrm{u}(T)$ is the number of unfrozen droplets at temperature T, N_o is the total number of droplets, A_deposit is the total area of the sample deposit on the hydrophobic glass cover slips, A_DFT is the area of the sample analyzed by the DFT, V is the volume of air sampled by the MOUDI, f_nu is a correction factor to account for changes in particle concentration across each MOUDI sample (because the DFT analyzes only a fraction of the entire sample), and f_ne is a correction factor to account for the uncertainty associated with the number of nucleation events in each

experiment following Koop et al. (1997). Additional details are available in Mason et al. (2015). Equation (1) takes into account the possibility of multiple INPs being contained in a single droplet using the method of Vali (1971). The total INP number concentration was found by summing the INP number concentrations over all analyzed MOUDI stages. Here we report INP data between -15 and -30 °C as few (1.3 %) of droplets froze at temperatures > -15 °C, and in some experiments all droplets were frozen at temperatures < -30 °C, which prohibited the calculation of INP number concentrations by Eq. (1). INP number concentrations have been adjusted to standard temperature and pressure.

2.3 Total and fluorescent aerosol measurements with sizes ≥ 0.5 μm

A model-4A waveband integrated bioaerosol sensor (WIBS-4A; Droplet Measurement Technologies, Boulder, CO, USA) was used to find both the total and fluorescent aerosol number concentrations with sizes ≥ 0.5 μm. Particles that enter the WIBS-4A first transect a continuous-wave 635 nm diode laser. The forward-scattered light from the continuous-wave laser is detected with a quadrant photomultiplier tube for the determination of particle size and asymmetry factor based on the signal intensity and asymmetry, respectively. The detected forward-scattered light also triggers excitation pulses from xenon lamps, the first at a wavelength of 280 nm and the second at 370 nm. The excitation pulses may lead to fluorescent emission from the particle, which is then collected in two wavelength ranges: 310–400 nm (short wavelength region) and 420–650 nm (long wavelength region). This results in sample information provided for each particle in three fluorescence channels: excitation at 280 nm, emission in the short wavelength region (FL1); excitation at 280 nm, emission in the long wavelength region (FL2); and excitation at 370 nm, emission in the long wavelength region (FL3). Detailed descriptions of the instrument can be found in Kaye et al. (2005), Gabey et al. (2010), and Healy et al. (2012a). The sample and

257 total flow rates of the WIBS-4A were 0.63 and 2.3 L min^{-1}, respectively, and number
258 concentrations have been adjusted to standard temperature and pressure.

259 The fluorescent channels used in the WIBS-4A allow for the detection of fluorophores
260 characteristic of biological activity. These fluorophores include the amino acid tryptophan, the
261 cofactor NAD(P)H, and the micronutrient riboflavin. While some non-biological species such as
262 soot, mineral dusts, polycyclic aromatic hydrocarbons, secondary organic aerosols, and humic-
263 like substances can produce a fluorescent signal (Pan et al., 1999; Sivaprakasam et al., 2004;
264 Bones et al., 2010; Gabey et al., 2011; Pöhlker et al., 2012; Lee et al., 2013), the number of
265 fluorescent particles is generally considered to be a lower limit to the number of primary
266 biological particles (Huffman et al., 2010, 2012; Pöhlker et al., 2012). In addition, fluorescence
267 microscopy measurements of samples collected during this field study show high concentrations
268 of fluorescent biological particles (see below). Therefore, fluorescent particles detected using the
269 WIBS-4A are hereafter referred to as fluorescent bioparticles.

270 Although the WIBS was used to determine the total and fluorescent aerosol number
271 concentrations with sizes ≥ 0.5 μm, it should be noted that the counting efficiency of the WIBS
272 for polystyrene latex spheres with particle diameters of 0.5 μm is roughly 50 % (Healy et al.,
273 2012b). Hence**,** concentration of particles reported here in the 0.5–1 μm size range should be
274 considered as lower limits.

275 **2.4 Fluorescence microscopy**

276 Aerosol samples were collected onto glass cover slips using a custom single-stage
277 impactor operating at a flow rate of 1.2 L min^{-1} with a 50 % cutoff aerodynamic diameter of 0.5
278 μm. Prior to sample collection, the substrates were coated with a thin layer of high viscosity
279 grease (Baysilone grease, Bayer, Germany) to reduce particle bounce.

Fluorescence microscopy images were taken on a BZ-9000 fluorescence microscope (Keyence, Inc., Osaka, Japan) equipped with a 120 W super high-compression mercury lamp and a 1.5 megapixel monochrome CCD camera. Images were obtained using the following fluorescence filters: OP-66834 DAPI-BP (λ_{ex} = 360/20 nm, $\lambda_{dichroic}$ = 400 nm, λ_{abs} = 460/25 nm), OP-66836 GFP-BP (λ_{ex} = 470/20 nm, $\lambda_{dichroic}$ = 495 nm, λ_{abs} = 535/25 nm), and OP-66838 TexasRed (λ_{ex} = 560/20 nm, $\lambda_{dichroic}$ = 595 nm, λ_{abs} = 630/30 nm). Filter specifications are given as wavelength of maximum absorbance or excitation and full width at half maximum (λ/FWHM).

2.5 Black carbon (BC) measurements

BC mass concentrations were measured using a multi-angle absorption photometer (MAAP model 5012; Thermo Scientific, Franklin, MA, USA). Detailed descriptions of the MAAP are available in Petzold et al. (2002), Petzold and Schönlinner (2004), and Petzold et al. (2005). Within the MAAP, particles are continuously collected on a glass fiber filter. The intensity of transmitted and forward-scattered light through the aerosol particle layer and filter matrix is measured by a photodetector located beneath the filter at a frequency of 1 Hz. The signal strength is attenuated by the presence of both light-absorbing particles and particles that cause backscattering. As the angular distribution of back-scattered light is related to the fraction of non-absorbing particles (Petzold and Schönlinner, 2004), four additional photodetectors located above the filter are used to quantify the non-absorbing component of the sample. The absorbance by the collected aerosol is then related to a mass of BC using a mass-specific absorption coefficient of 6.6 $m^2 g^{-1}$. Mass concentrations have been adjusted to standard temperature and pressure.

Non-BC material such as mineral dusts and brown carbon can also absorb 670 nm

303 wavelength light used in the MAAP, albeit with smaller absorption coefficients than BC (Yang
304 et al., 2009). We follow the recommendation of Petzold et al. (2013) for BC data derived from
305 optical absorption methods and hereafter refer to MAAP data as measurements of equivalent
306 black carbon (eBC).

307 **2.6 Tracers of anthropogenic aerosols**

308 Measurements of CO, NO_x, and SO_2 were used to identify anthropogenic contributions to
309 the sampled air masses as sources of these gases include fossil fuel combustion and biomass
310 burning (Galanter et al., 2000; Gadi et al., 2003; United States Environmental Protection
311 Agency, 2014). CO concentrations were monitored using a Thermo Fisher Scientific 48i-TL, an
312 absorbance-based analyzer using infrared light at a wavelength of 4.6 μm. NO_x concentrations
313 were monitored using chemiluminescence with a Thermo Fisher Scientific 42i. This instrument
314 first converts NO_2 to NO, which then reacts with ozone to produce luminescence of intensity in
315 proportion to the level of NO_x. A Teledyne API T100U, using fluorescence emitted by SO_2
316 under excitation by ultraviolet light, monitored SO_2 concentrations. Data were collected for each
317 instrument at a frequency of 1 min^{-1}.

318 **2.7 Ion measurements**

319 Size-resolved aerosol samples were collected on Teflon® filters (Pall Corporation, Port
320 Washington, NY, USA) using a second MOUDI (model 110R). Samples were collected on the
321 inlet, stage 1, and stages 7–10 of the MOUDI with stages 2–6 being removed prior to collection.
322 The flow rate through the MOUDI was on average 24 L min^{-1}, resulting in a collected size range
323 of 0.068 μm to > 20 μm (50 % cutoff aerodynamic diameter). Collection times ranged from
324 approximately 45–49 hours and samples were stored at 4 °C for a period of one month before
325 analysis.

Mass concentrations of sodium and methanesulfonic acid (MSA) were found using cationic and anionic chromatography following the method of Phinney et al. (2006). Briefly, filters were extracted with sonication in 10 mL of deionized water for 1 hour, and samples were analyzed with a Dionex DX600 ion chromatograph using an AS11-HC column and a CS12 column for anions and cations, respectively. Filter blanks were measured to be below the limit of detection for both analytes. Mass concentrations were adjusted to standard temperature and pressure.

2.8 Back trajectories

Back trajectories spanning a period of 72 hours were calculated for each sampling period using the Hybrid Single-Particle Lagrangian Integrated Trajectory (HYSPLIT4) model of the National Oceanographic and Atmospheric Administration and the GDAS1 meteorological data archive (Draxler and Rolph, 2014). To determine if the air mass changed during a sampling period, back trajectories were initiated at the beginning of the sampling period and every 2 hours until the end of the sampling period from a height of 5.5 m. Trajectories were also initiated from a height of 50 and 150 m agl for cases where the trajectories approached ground level. The conclusions in this manuscript were not sensitive to the height at which the back trajectories were initiated.

Back trajectories were used to assign each sampling period to one of four general air mass categories: (i) *coastal NW* where boundary layer air (defined here as an altitude below 1000 m) has traversed land northwest of the sampling site during its approach; (ii) *coastal SE* where boundary layer air has traversed land southeast of the sampling site during its approach; (iii) *Pacific Ocean* where boundary layer air has approached directly from the ocean and has not encountered land prior to arrival at the sampling site; and (iv) *free troposphere* where the air

mass has spent more than 50 % of the 72 hour back trajectory in the free troposphere. In four sampling periods, back trajectories initiated at different times in the sampling period indicated that the air mass changed during sampling, such as a change in the predominant altitude of the air mass from the free troposphere to the marine boundary layer. In these situations, the air mass category to which the majority of the back trajectories belonged was selected as the air mass category of the sample.

3. Results and discussion

3.1 Back trajectories and the dependence of INP concentrations on air mass classification

Seventy-two hour back trajectories initiated at the midpoint of each INP sampling period are shown in Fig. 2. The back trajectories indicate that 88 % of the air masses sampled spent the majority of their 72 hours prior to reaching the site over the Pacific Ocean within the marine boundary layer (est. < 1000 m). Furthermore, air masses approached the sampling site from an onshore direction with minimal flow over land apart from coastal regions. Average local wind directions of 89° to 297° during INP sampling support this finding. In Fig. S1 of the Supplement, the back trajectories shown in Fig. 2 are color-coded by the classification of the air mass.

Shown in Fig. 3 is the number concentration of INPs as a function of time, color-coded by the classification of the air mass. There is no obvious trend between INP number concentrations and air mass type at temperatures between -15 and -25 °C. At -30 °C, INP number concentrations associated with air masses from the coastal SE (red points) appear to be higher than INP number concentrations associated with other air masses, but the statistics are low for the coastal SE air masses, especially at -30 °C. Figure 4 shows that the mean values for the different air mass types vary by less than a factor of 2.6. We conclude that INP number

372 concentrations did not exhibit a strong dependence on the type of air mass sampled. The
373 correlation analysis presented in Sects. 3.2–3.5 uses the entire dataset (i.e. the data were not
374 differentiated based on air mass type). We further explore the dependence on air mass type in
375 Sect. 3.6.

376 **3.2 Are biological particles a major source of ice nuclei?**

377 To investigate if biological particles are an important source of INPs at the coastal site,
378 we determined correlations between INPs and fluorescent bioparticles. In the following
379 correlation analysis, WIBS-4A data are limited to particle sizes of 10 μm or smaller to better
380 match the size range of the MOUDI-DFT. The correlation coefficients (R) of linear fits to the
381 data are presented in Table 1 with correlation plots at a freezing temperature of -25 °C shown in
382 Fig. 5 and plots at -15, -20, and -30 °C given in the Supplement. Here we use the scheme of
383 Dancey and Reidy (2011) where correlations with an R value of 0.1–0.3, 0.4–0.6, and 0.7–0.9 are
384 classified as weak, moderate, and strong, respectively. In the discussion, correlations with
385 statistical significance (P value < 0.05) are emphasized.

386 With values of R between 0.74 and 0.83, INP number concentrations are strongly
387 correlated with the number concentrations of fluorescent bioparticles for INPs active between -
388 15 and -25 °C (Figs. 5a and S3, Table 1). At these temperatures, fluorescent bioparticles have the
389 largest correlation coefficients with INPs compared to all of the other parameters investigated.
390 This suggests that biological particles are an important component of the INP population. Using
391 similar fluorescence techniques, others have also noted strong correlations between INPs and
392 primary biological particles during ambient measurements (Prenni et al., 2009, 2013; Huffman et
393 al., 2013; Tobo et al., 2013).

394 To further investigate the relationship between biological particles and INPs, we

compared the size distributions of INPs with the size distributions of total particles and fluorescent bioparticles, using samples where all three measurements were available. Shown in Fig. 6a–d are the average number concentrations of INPs as a function of particle size for droplet freezing temperatures ranging from -15 to -30 °C. The shapes of all four INP size distributions were nearly identical with a single mode at an aerodynamic diameter of 3.2–5.6 μm.

Also shown in Fig. 6 are the average size distributions of total particles and fluorescent bioparticles as measured with the WIBS-4A over the size range of 0.5–10 μm. As mentioned in Sect. 2.3, due to the decrease in WIBS counting efficiency at particle sizes below approximately 0.7 μm (Healy et al., 2012b), the number concentration of particles sized 0.5–1.0 μm should be considered a lower limit.

The size distribution of total particles (Fig. 6e) was found to be unimodal with the mode at 0.5–1.0 μm. Fluorescent bioparticles were bimodally distributed (Fig. 6f) with one mode at 1.8–3.2 μm and another at 0.5–1.0 μm. Figure 6 illustrates that the size distributions of INPs are more closely related to the size distribution of fluorescent bioparticles than total particles, suggesting that biological particles may have had a greater contribution to the INP population than non-biological particles.

In addition to the WIBS-4A, the presence of biological material in sampled air was verified by fluorescence microscopy. Images of a sample collected on August 11, 2013 are shown in Fig. 7 as an example. The fraction of particles exhibiting fluorescence on this day based on the WIBS-4A was close to the campaign average value; 7.1 % versus an average of 7.8 %. The image here shows a sample containing many biological particles, identified by their blue color which is characteristic of biological fluorophores such as proteins and coenzymes (Pöhlker et al., 2012). Most of these biological particles had a similar morphology with an ellipsoidal

418 shape, approximately 11.9 μm in length × 4.1 μm in width, and multi-nucleation with three
419 septa. Morphologically, many of these appear to be fungal macroconidia, consistent with the
420 physical attributes of ascospores (Carlile et al., 2001; Maheshwari, 2005; Leslie and Summerell,
421 2006; Webster and Weber, 2007). Fungal spores can be ice-active at the temperatures used here
422 (Jayaweera and Flanagan, 1982; Pouleur et al., 1992; Tsumuki et al., 1992; Richard et al., 1996;
423 Iannone et al., 2011; Haga et al., 2013, 2014; Fröhlich-Nowoisky et al., 2015), and the size of the
424 bioparticles observed in Fig. 7 (an estimated aerodynamic diameter of 4.8 μm assuming a prolate
425 spheroid shape and unit density) matches the mode in the INP size distributions of Fig. 6.
426 Predicting the optical diameter that the WIBS-4A would measure for such a particle is difficult,
427 but it is reasonable that they could be detected as slightly larger or smaller depending on the axis
428 upon which the incident light impinges.

429 **3.3 Is black carbon a major source of ice nuclei?**

430 Sources of BC at the sampling site include local marine ship traffic. Atmospheric size
431 distributions obtained at other locations demonstrate that most BC particles are smaller than 1
432 μm (Schwarz et al., 2008, 2013; Schroder et al., 2015). As is shown in Fig. 6, the majority of
433 INPs identified here were larger than 1 μm at all of the temperatures studied. It is therefore likely
434 that BC particles were not the major source of INPs at the sampling site. As correlations between
435 INPs and eBC are moderate at -15 to -25 °C (R = 0.47–0.60, Table 1), we also investigated
436 correlations between INPs and the anthropogenic tracers CO, NO_x, and SO_2. The correlations
437 between INPs and CO, NO_x, and SO_2 are not statistically significant (see Table S2 of the
438 Supplement), further suggesting that BC was not a major INP source.

439 **3.4 Are particles from the ocean a major source of ice nuclei?**

440 Situated in a region of high oceanic primary productivity (Whitney et al., 2005; Ribalet et

al., 2010) with onshore winds, particles of marine origin are a potential source of INPs at the sampling site. Therefore, correlations between INP number concentrations and tracers of marine aerosols and marine biological activity were explored. Since primary marine aerosols are ejected from the ocean by the bursting of entrained bubbles (Blanchard and Woodcock, 1957; Blanchard, 1963, 1989; Andreas, 1998), sodium was used as a tracer of primary particles from the ocean. The strength of correlations between INPs and sodium are given in Table 1. Although the correlations range from weakly-to-moderately negative to strongly positive, the large *P* values (0.20 or greater) indicate that the results are not statistically significant. Due in part to the long sampling times required for the sodium measurements, only three to six data points were available for the sodium correlation analysis.

MSA is often used as a marker for marine biological productivity (Saltzman et al., 1986; Savoie et al., 1994; Sorooshian et al., 2009; Gaston et al., 2010; Becagli et al., 2013) because it is chemically stable and its precursor, dimethylsulfide, is produced by primary biological activity in the ocean (Andreae et al., 1985; Charlson et al., 1987; Keller, 1989; Bates et al., 1992; Kettle et al., 1999). As INP number concentrations are closely correlated to bioparticles at warmer droplet freezing temperatures, one may expect correlations of a similar magnitude between INPs and MSA if the marine environment was indeed acting as an important source of biological INPs. As is shown in Table 1, no statistically significant correlations are found as *P* values are large (0.15-0.50).

Finally, correlations between wind speed and INP number concentration were investigated using wind speed data from both the site and an offshore buoy. As the dominant source of bubble entrainment in the oceans is breaking waves (O'Dowd and de Leeuw, 2007), the rate of sea-spray production is dependent in part on wind speed. For this correlation, wind

speed was first raised to the power of 3.41 using the power law of Monahan and Muircheartaigh (1980) that relates whitecap coverage to wind speed. The correlations found at -30 °C are statistically significant (P value < 0.05), but the magnitude of the correlation coefficients is only moderate (R = 0.48–0.55; see Table 1). The average wind speed during INP sampling exceeded the onset speed for whitecap formation, approximately 4 m s^{-1} (O'Dowd and de Leeuw, 2007), in only 47 and 56 % of samples when using the lighthouse and buoy data, respectively, and daily observations at the site noted infrequent wave activity. Furthermore, some of the highest INP concentrations were found when the wind speed was less than 4 m s^{-1}. The correlation between local wind direction and INP concentrations was also weak (R ranged from -0.19 to -0.32; not shown).

All correlations between INPs and parameters indicative of marine aerosols and marine biological activity are either moderate at best or not statistically significant. For these reasons, correlations involving sodium, MSA, and wind speed do not provide strong evidence that marine particles were a major contributor to the INP population. Recent measurements have shown the presence of INPs in the sea surface microlayer (Wilson et al., 2015). Our measurements do not contradict these findings since we do not rule out the ocean as a source of INPs. One possibility is that biological INPs released by local vegetation were present in sufficient numbers at this site to overwhelm the presence of any INPs from the ocean.

3.5 What is the major source of ice nuclei active at -30 °C?

At warmer droplet freezing temperatures (-15 to -25 °C), the strongest correlations are observed between number concentrations of fluorescent bioparticles and INPs. In contrast, at -30 °C the strength of correlations between INPs and fluorescent bioparticles and INPs and total particles > 0.5 μm in diameter are equal (R = 0.66; Table 1). It is therefore likely that both

487 biological and non-biological particles were important sources of INPs active at -30 °C. Good
488 correlations between INPs and total particles > 0.5 μm have also been observed in several other
489 field studies (e.g. DeMott et al., 2010; Chou et al., 2011; Field et al., 2012; Prenni et al., 2013;
490 Tobo et al., 2013; Jiang et al., 2015).

491 Since the INP size distributions of Fig. 6 and the correlations of Table 1 do not provide
492 strong evidence of BC particles or the ocean being a major source of INPs active at -30 °C, it is
493 possible that mineral dust was a major source of INPs as mineral dust particles are known to
494 efficiently nucleate ice at this temperature (e.g. DeMott et al., 2003; Cziczo et al., 2004; Field et
495 al., 2006; Möhler et al., 2006; Marcolli et al., 2007; Zimmermann et al., 2008; Klein et al., 2010;
496 Niedermeier et al., 2010; Chou et al., 2011; Atkinson et al., 2013; Yakobi-Hancock et al., 2013;
497 Wheeler et al., 2015). The size distribution of INPs did not drastically change between -25 and -
498 30 °C (Fig. 6c and d), and the dominant mode in the surface area distribution of airborne mineral
499 dust (Maring et al., 2003) can occur at approximately the same size range as biological INPs
500 (Després et al., 2012). While in a very different ecosystem and climatic region, Prenni et al.
501 (2009) noted that the relative contribution of mineral dust particles to the total number of INPs in
502 the Amazon region increased as ice nucleation temperature decreased. Only below -27 °C did the
503 amount of mineral dust significantly influence the number of INPs, while above this temperature
504 most INPs were biological (Prenni et al., 2009). Ten-day back trajectories initiated at the
505 midpoint of each INP sampling period are available in Fig. S2 of the Supplement. None of the
506 trajectories pass over major arid regions in Asia or Africa; however, this does not rule out
507 mineral dust or soils as a source of INPs in our measurements.

508 **3.6 Do the potential sources of ice nuclei change with air mass classification?**

In the preceding sections we did not differentiate data based on air mass classification. Here we present correlations within each of the four air mass categories introduced in Sect. 2.8 to investigate if the major sources of INPs vary with air mass type. The correlations for each air mass type are given in Table 2. Correlations involving sodium and MSA are not included due to insufficient data, and only statistically significant correlations will be discussed ($P < 0.05$).

The general trends presented in Table 1 for the undifferentiated data are also found in Table 2 for the various air mass categories. In coastal NW, Pacific Ocean, and free tropospheric air masses, INP number concentrations are well correlated to those of fluorescent bioparticles at temperatures between -15 and -25 °C with R values ranging from 0.64 to 0.99 (an average of 0.89), and in free tropospheric air masses a very strong correlation is also found at -30 °C (R = 1.00). In most cases, these are the strongest correlations noted at a given temperature. This again suggests that many INPs may have been biological.

In coastal NW and free tropospheric air masses, INPs and total particles are also closely correlated. These correlations are strong in the case of coastal NW air masses at ice activation temperatures of -15 to -25 °C (R = 0.70–0.85) and very strong in air masses from the free troposphere between -20 and -30 °C (R = 0.98–0.99). The correlation coefficients are significantly greater than those found in the undifferentiated data of Table 1. With the average fraction of particles that exhibited fluorescence in these air masses being close to the campaign average, the good correlations with total particles suggest that non-biological INPs such as mineral dust may have also contributed to the INP population.

Correlations of INPs with eBC are strong (R = 0.71–0.84) at -25 °C and above in coastal NW air masses and very strong (R = 0.99) at -15 °C in air masses from the free troposphere. Correlations of INPs with CO and SO_2 in these air masses are also moderate to very strong in

some cases (see Table S3 of the Supplement). However, more than 84 and 100 % of INPs active at these temperatures were larger than 1 μm in size in air masses from the coastal NW and the free troposphere, respectively. Vegetation NW of the sampling site closely follows that of the region, and potential sources of supermicron INPs from the coastal NW include forests of coastal western hemlock. Given the dominance of supermicron INPs in these two air mass types, it is unlikely that BC was an important source of INPs.

3.7 Can existing parameterizations accurately predict measured INP concentrations?

Empirical parameterizations have been developed to predict ice nucleation in atmospheric models. Here we investigate whether or not a number of these parameterizations are consistent with the current measurements. In total we tested six different parameterizations: those of Fletcher (1962), hereafter F62; Cooper (1986), hereafter C86; Meyers et al. (1992), hereafter M92; DeMott et al. (2010), hereafter D10; and two from Tobo et al. (2013), hereafter $T13_{total}$ and $T13_{fluorescent}$. Details on these parameterizations are given in the Supplement.

In Fig. 8 we compare measured INP number concentrations with predicted INP number concentrations based on the parameterizations discussed above. The parameterizations of D10, $T13_{total}$ and $T13_{fluorescent}$ require knowledge of either total particle or fluorescent bioparticle number concentrations with sizes > 0.5 μm. Here we use the data from the WIBS-4A over its full size range (0.5–23.7 μm) to better match the sampling conditions used in D10 and T13. Note that the parameterization of $T13_{fluorescent}$ based on fluorescent bioparticle number concentrations was formulated using measurements from an ultraviolet aerodynamic particle sizer (UV-APS), whereas this study uses a WIBS-4A. As noted in Healy et al. (2014), there may be discrepancies between the number concentrations of fluorescent bioparticles detected by the UV-APS and WIBS-4A. With more fluorescent channels and more sensitive electronics, the WIBS-4A may

555 probe different fluorophores than the UV-APS, thus detecting greater concentrations of
556 fluorescent bioparticles and in turn leading to greater predicted INP number concentrations.
557 Also, the INP number concentrations measured by the MOUDI-DFT are for particle sizes of
558 0.18–10 μm, whereas the INP measurements used to formulate the parameterizations of M92,
559 D10, and T13 were for particles ≤ 3, ≤ 1.6, and ≤ 2.4 μm, respectively. As a result, when
560 reporting measured INP number concentrations in Fig. 8 we limit the MOUDI-DFT data to
561 particle sizes that overlap with those used to formulate the parameterizations (see the
562 Supplement for details).

563 It is evident in Fig. 8 that none of the parameterizations are able to consistently predict
564 the measured INP number concentrations within a factor or 5 over the entire temperature range
565 investigated. The most accurate parameterization is that of C86 (Fig. 8b), predicting 25 % and 57
566 % of the INP number concentrations within a factor of 2 and 5, respectively, of the solid 1:1 line.
567 While the C86 parameterization works reasonably well at temperatures of -15 to -25 °C, at lower
568 temperatures it becomes increasingly inaccurate, possibly due to it being applied outside the
569 temperature range over which it was developed (-5 to -25 °C).

570 The parameterizations of D10, $T13_{total}$ and $T13_{fluorescent}$ incorporate measurements of total
571 particles or fluorescent bioparticles, but are found to be poor predictors of the values measured in
572 this study as on average only 41% of INP number concentrations are predicted within a factor of
573 5 (Fig. 8d–f). A number of datasets from diverse locations were used in the development of the
574 D10 parameterization, but those with a strong marine influence were not included because sea
575 salt is not known to be an efficient ice nucleus under the conditions investigated (immersion
576 freezing at temperatures above -35 °C). Given the proximity of our sampling site to the Pacific
577 Ocean (Fig. 1) and the back trajectories of the sampled air masses (Fig. 2), a marine influence in

578 our samples may contribute to the somewhat poor performance of the D10 parameterization and
579 the over-estimation of INPs shown in Fig. 8d. The $T13_{total}$ and $T13_{fluorescent}$ parameterizations
580 were developed using data from a forested site in Colorado. Differences in the composition,
581 concentration, and ice-nucleating ability of both biological and non-biological particles between
582 the continental forest of T13 and the coastal site of this study may have contributed to the
583 inaccuracy of the $T13_{total}$ and $T13_{fluorescent}$ parameterizations (Fig. 8e–f).

584 Figure 8 suggests that additional measurements of INPS in other environments, times of
585 year, and altitudes are needed to further test and improve current empirical parameterizations of
586 INPs. The results presented in Fig. 8 also indicate that the application of INP parameterizations
587 to locations dissimilar to that of the original study used to generate the parameterizations should
588 be done with care.

589 **4. Summary and conclusions**

590 The number concentrations of 0.18–10 μm INPs active in the immersion mode were
591 determined at a coastal site in Western Canada during the summer of 2013 as part of the
592 NETCARE project. We investigated the strength of linear correlations between these INP values
593 and measurements of total particles, fluorescent bioparticles, eBC, sodium, MSA, and wind
594 speed and also compared their size distributions where these measurements were available. We
595 found that (1) biological particles, possibly from local vegetation, were likely the major source of
596 ice nuclei at freezing temperatures between -15 and -25 °C; (2) non-biological particles such as
597 mineral dust may also have had an important contribution to the population of INPs active at -30
598 °C; (3) the prevalence of supermicron INPs makes BC particles an unlikely source of ice nuclei;
599 and (4) there was no evidence of marine particles being a significant source of ice nuclei,
600 although the ocean as a source of INPs cannot be ruled out. One possibility is that biological

INPs released by nearby vegetation were present in sufficient numbers at this site to overwhelm the presence of any INPs from the ocean.

Six empirical parameterizations of ice nucleation for use in atmospheric models were tested to determine the accuracy with which they predict INP number concentrations at this coastal site. Overall, none of the parameterizations were found to be suitable, predicting only 1 to 57 % of INPs within a factor of 5 of the measured value. This highlights the need for the development of INP parameterizations that are appropriate for this complex environment.

In this paper we assumed that particles were externally mixed. In future studies it would be useful to include mixing state measurements together with studies similar to those presented here to quantify the extent of external versus internal mixing. In addition, studies that identify INPs followed by chemical composition measurements of these particles by electron microscopy (e.g. Knopf et al., 2014) or fluorescence microscopy would be useful to supplement the information gained from correlation analyses of collocated instruments.

Acknowledgements

The authors thank K. Bach, O. Greiner, J. Hansen, A. Klady, K. Love, D. Lovrity, T. Mittertreiner, R. Neagu, P. Padhiar for designing and constructing the NETCARE mobile laboratory used in this study, A. Chivulescu for assistance with ion chromatography measurements, D. O'Connor for assistance analyzing and interpreting WIBS-4A measurements, and L. A. Miller for helpful discussions. The sampling site at Amphitrite Point is located at a Coast Guard station and we would like to thank the Department of Fisheries and Oceans and all the staff at the site for their help. The site is jointly supported and maintained by Environment Canada, the British Columbia Ministry of Environment, and Metro Vancouver. The Natural Sciences and Engineering Research Council of Canada supported this research through its

Climate Change and Atmospheric Research program. The authors gratefully acknowledge the NOAA Air Resources Laboratory (ARL) for the provision of the HYSPLIT transport and dispersion model and READY website (http://www.ready.noaa.gov) used in this publication. J. A. Huffman and J. Li acknowledge internal faculty support from the Division of Natural Sciences and Math and PROF grant support from the Office of Research and Sponsored Programs at the University of Denver.

References

Alpert, P. A., Aller, J. Y. and Knopf, D. A.: Ice nucleation from aqueous NaCl droplets with and without marine diatoms, Atmos. Chem. Phys., 11, 5539–5555, doi:10.5194/acp-11-5539-2011, 2011.

Andreae, M. O., Ferek, R. J., Bermond, F., Byrd, K. P., Engstrom, R. T., Hardin, S., Houmere, P. D., LeMarrec, F., Raemdonck, H. and Chatfield, R. B.: Dimethyl sulfide in the marine atmosphere, J. Geophys. Res., 90, 12891–12900, doi:10.1029/JD090iD07p12891, 1985.

Andreas, E. L.: A New Sea Spray Generation Function for Wind Speeds up to 32 m s^{-1}, J. Phys. Oceanogr., 28, 2175–2184, 1998.

Atkinson, J. D., Murray, B. J., Woodhouse, M. T., Whale, T. F., Baustian, K. J., Carslaw, K. S., Dobbie, S., O'Sullivan, D. and Malkin, T. L.: The importance of feldspar for ice nucleation by mineral dust in mixed-phase clouds, Nature, 498, 355–358, doi:10.1038/nature12278, 2013.

Augustin, S., Wex, H., Niedermeier, D., Pummer, B., Grothe, H., Hartmann, S., Tomsche, L., Clauss, T., Voigtländer, J., Ignatius, K. and Stratmann, F.: Immersion freezing of birch pollen washing water, Atmos. Chem. Phys., 13, 10989–11003, doi:10.5194/acp-13-10989-2013, 2013.

Austin, M. A., Buffet, D. A., Nicholson, D. J. and Scudder, G. G. E.: Taking Natures Pulse: The Status of Biodiversity in British Columbia, Biodiversity BC, Victoria, available at: http://www.biodiversitybc.org (last access: 10 October 2014), 2008.

Baker, M. B.: Cloud Microphysics and Climate, Science, 276, 1072–1078, doi:10.1126/science.276.5315.1072, 1997.

Bates, T. S., Calhoun, J. A. and Quinn, P. K.: Variations in the methanesulfonate to sulfate molar ratio in submicrometer marine aerosol particles over the South Pacific Ocean, J. Geophys. Res. Ocean., 97, 9859–9865, doi:10.1029/92JD00411, 1992.

Becagli, S., Lazzara, L., Fani, F., Marchese, C., Traversi, R., Severi, M., di Sarra, A., Sferlazzo, D., Piacentino, S., Bommarito, C., Dayan, U. and Udisti, R.: Relationship between methanesulfonate (MS^-) in atmospheric particulate and remotely sensed phytoplankton activity in

oligo-mesotrophic central Mediterranean Sea, Atmos. Environ., 79, 681–688, doi:10.1016/j.atmosenv.2013.07.032, 2013.

Blanchard, D. C.: The electrification of the atmosphere by particles from bubbles in the sea, Prog. Oceanogr., 1, 73–202, doi:10.1016/0079-6611(63)90004-1, 1963.

Blanchard, D. C.: The ejection of drops from the sea and their enrichment with bacteria and other materials: A review, Estuaries, 12, 127–137, doi:10.2307/1351816, 1989.

Blanchard, D. C. and Woodcock, A. H.: Bubble formation and modification in the sea and its meteorological significance, Tellus, 9, 145–158, doi:10.1111/j.2153-3490.1957.tb01867.x, 1957.

Bones, D. L., Henricksen, D. K., Mang, S. A., Gonsior, M., Bateman, A. P., Nguyen, T. B., Cooper, W. J. and Nizkorodov, S. A.: Appearance of strong absorbers and fluorophores in limonene-O_3 secondary organic aerosol due to NH_4^+-mediated chemical aging over long time scales, J. Geophys. Res., 115, D05203, doi:10.1029/2009JD012864, 2010.

Boucher, O., Randall, D., Artaxo, P., Bretherton, C., Feingold, G., Foster, P., Kerminen, V.-M., Kondo, Y., Liao, H., Lohmann, U., Rasch, P., Satheesh, S. K., Sherwood, S., Stevens, B. and Boucher, O., Randall, D., Artaxo, P., Bretherton, C., Feingold, G., Foster, P., Kerminen, V.-M., Kondo, Y., Liao, H., Lohmann, U., Rasch, P., Satheesh, S. K., Sherwood, S., Stevens, B. and Zhang, X. Y.: Clouds and Aerosols, in Climate Change 2013: The Physical Science Basis. Contribution of Working Group I to the Fifth Assessment Report of the Intergovernmental Panel on Climate Change, edited by T. F. Stocker, D. Qin, G.-K. Plattner, M. Tignor, S. K. Allen, J. Boschung, A. Nauels, Y. Xia, V. Bex, and P. M. Midgley, Cambridge University Press, Cambridge, United Kingdom and New York, NY, USA, 2013.

Broadley, S. L., Murray, B. J., Herbert, R. J., Atkinson, J. D., Dobbie, S., Malkin, T. L., Condliffe, E. and Neve, L.: Immersion mode heterogeneous ice nucleation by an illite rich powder representative of atmospheric mineral dust, Atmos. Chem. Phys., 12, 287–307, doi:10.5194/acp-12-287-2012, 2012.

Brooks, S. D., Suter, K. and Olivarez, L.: Effects of Chemical Aging on the Ice Nucleation Activity of Soot and Polycyclic Aromatic Hydrocarbon Aerosols, J. Phys. Chem. A, 118, 10036–10047, doi:10.1021/jp508809y, 2014.

Burrows, S. M., Hoose, C., Pöschl, U. and Lawrence, M. G.: Ice nuclei in marine air: biogenic particles or dust?, Atmos. Chem. Phys., 13, 245–267, doi:10.5194/acp-13-245-2013, 2013.

Carlile, M. J., Watkinson, S. C. and Gooday, G. W.: The Fungi, Second Edi., Academic Press, London, United Kingdom and San Diego, CA, USA, 2001.

Charlson, R. J., Lovelock, J. E., Andreae, M. O. and Warren, S. G.: Oceanic phytoplankton, atmospheric sulphur, cloud albedo and climate, Nature, 326, 655–661, doi:10.1038/326655a0, 1987.

Chou, C., Stetzer, O., Weingartner, E., Jurányi, Z., Kanji, Z. A. and Lohmann, U.: Ice nuclei properties within a Saharan dust event at the Jungfraujoch in the Swiss Alps, Atmos. Chem. Phys., 11, 4725–4738, doi:10.5194/acp-11-4725-2011, 2011.

Christner, B. C., Morris, C. E., Foreman, C. M., Cai, R. and Sands, D. C.: Ubiquity of Biological Ice Nucleators in Snowfall, Science, 319, 1214, doi:10.1126/science.1149757, 2008.

697 Conen, F., Morris, C. E., Leifeld, J., Yakutin, M. V and Alewell, C.: Biological residues define
698 the ice nucleation properties of soil dust, Atmos. Chem. Phys., 11, 9643–9648, doi:10.5194/acp-
699 11-9643-2011, 2011.

700 Cooper, W. A.: Ice initiation in natural clouds, Meteor. Mon., 21, 29–32, doi:10.1175/0065-
701 9401-21.43.29, 1986.

702 Corbin, J. C., Rehbein, P. J. G., Evans, G. J. and Abbatt, J. P. D.: Combustion particles as ice
703 nuclei in an urban environment: Evidence from single-particle mass spectrometry, Atmos.
704 Environ., 51, 286–292, doi:10.1016/j.atmosenv.2012.01.007, 2012.

705 Costa, T. S., Gonçalves, F. L. T., Yamasoe, M. A., Martins, J. A. and Morris, C. E.: Bacterial ice
706 nuclei impact cloud lifetime and radiative properties and reduce atmospheric heat loss in the
707 BRAMS simulation model, Environ. Res. Lett., 9, 084020, doi:10.1088/1748-9326/9/8/084020,
708 2014.

709 Cozic, J., Mertes, S., Verheggen, B., Cziczo, D. J., Gallavardin, S. J., Walter, S., Baltensperger,
710 U. and Weingartner, E.: Black carbon enrichment in atmospheric ice particle residuals observed
711 in lower tropospheric mixed phase clouds, J. Geophys. Res., 113, D15209,
712 doi:10.1029/2007JD009266, 2008.

713 Creamean, J. M., Suski, K. J., Rosenfeld, D., Cazorla, A., DeMott, P. J., Sullivan, R. C., White,
714 A. B., Ralph, F. M., Minnis, P., Comstock, J. M., Tomlinson, J. M. and Prather, K. A.: Dust and
715 Biological Aerosols from the Sahara and Asia Influence Precipitation in the Western U.S.,
716 Science, 339, 1572–1578, doi:10.1126/science.1227279, 2013.

717 Cziczo, D. J., Froyd, K. D., Hoose, C., Jensen, E. J., Diao, M., Zondlo, M. A., Smith, J. B.,
718 Twohy, C. H. and Murphy, D. M.: Clarifying the Dominant Sources and Mechanisms of Cirrus
719 Cloud Formation, Science, 340, 1320–1324, doi:10.1126/science.1234145, 2013.

720 Cziczo, D. J., Murphy, D. M., Hudson, P. K. and Thomson, D. S.: Single particle measurements
721 of the chemical composition of cirrus ice residue during CRYSTAL-FACE, J. Geophys. Res.,
722 109, D04201, doi:10.1029/2003JD004032, 2004.

723 Dancey, C. P. and Reidy, J.: Statistics Without Maths for Psychology, Pearson Education
724 Limited, Essex, England, 2011.

725 DeMott, P. J., Hill, T. C. J., McCluskey, C. S., Prather, K. A., Collins, D. B., Sullivan, R. C.,
726 Ruppel, M. J., Mason, R. H., Irish, V. E., Lee, T., Hwang, C. Y., Rhee, T. S., Snider, J. R.,
727 McMeeking, G. R., Dhaniyala, S., Lewis, E. R., Wentzell, J., Abbatt, J. P. D., Lee, C., Sultana,
728 C. M., Ault, A. P., Axson, J. I., Martinez, M. D., Venero, I., Figueroa, G. S., Stokes, M. D.,
729 Deane, G. B., Mayol-Bracero, O. L., Grassian, V. H., Bertram, T. H., Bertram, A. K., Moffett, B.
730 F. and Franc, G. D.: Sea spray aerosol as a unique source of ice nucleating particles, submitted,
731 2015.

732 DeMott, P. J., Petters, M. D., Prenni, A. J., Carrico, C. M., Kreidenweis, S. M., Collett Jr., J. L.
733 and Moosmüller, H.: Ice nucleation behavior of biomass combustion particles at cirrus
734 temperatures, J. Geophys. Res., 114, D16205, doi:10.1029/2009JD012036, 2009.

735 DeMott, P. J., Prenni, A. J., Liu, X., Kreidenweis, S. M., Petters, M. D., Twohy, C. H.,
736 Richardson, M. S., Eidhammer, T. and Rogers, D. C.: Predicting global atmospheric ice nuclei
737 distributions and their impacts on climate, P. Natl. Acad. Sci. USA, 107, 11217–11222,
738 doi:10.1073/pnas.0910818107, 2010.

739 DeMott, P. J., Sassen, K., Poellot, M. R., Baumgardner, D., Rogers, D. C., Brooks, S. D., Prenni,
740 A. J. and Kreidenweis, S. M.: African dust aerosols as atmospheric ice nuclei, Geophys. Res.
741 Lett., 30, 1732, doi:10.1029/2003GL017410, 2003.

742 Després, V. R., Huffman, J. A., Burrows, S. M., Hoose, C., Safatov, A. S., Buryak, G., Fröhlich-
743 Nowoisky, J., Elbert, W., Andreae, M. O., Pöschl, U. and Jaenicke, R.: Primary biological
744 aerosol particles in the atmosphere: a review, Tellus B, 64, 15598,
745 doi:10.3402/tellusb.v64i0.15598, 2012.

746 Diehl, K., Matthias-Maser, S., Jaenicke, R. and Mitra, S. K.: The ice nucleating ability of pollen:
747 Part II. Laboratory studies in immersion and contact freezing modes, Atmos. Res., 61, 125–133,
748 doi:10.1016/S0169-8095(01)00132-6, 2002.

749 Diehl, K. and Mitra, S. K.: A laboratory study of the effects of a kerosene-burner exhaust on ice
750 nucleation and the evaporation rate of ice crystals, Atmos. Environ., 32, 3145–3151,
751 doi:10.1016/S1352-2310(97)00467-6, 1998.

752 Diehl, K., Quick, C., Matthias-Maser, S., Mitra, S. K. and Jaenicke, R.: The ice nucleating ability
753 of pollen: Part I. Laboratory studies in deposition and condensation freezing modes, Atmos. Res.,
754 58, 75–87, doi:10.1016/S0169-8095(01)00091-6, 2001.

755 Draxler, R. R. and Rolph, G. D.: HYSPLIT (HYbrid Single-Particle Lagrangian Integrated
756 Trajectory) Model access via NOAA ARL READY Website, available at:
757 http://ready.arl.noaa.gov/HYSPLIT.php (last access: 27 May 2014), NOAA Air Resources
758 Laboratory, Silver Spring, MD, 2014.

759 Dymarska, M., Murray, B. J., Sun, L., Eastwood, M. L., Knopf, D. A. and Bertram, A. K.:
760 Deposition ice nucleation on soot at temperatures relevant for the lower troposphere, J. Geophys.
761 Res., 111, D04204, doi:10.1029/2005JD006627, 2006.

762 Ebert, M., Worringen, A., Benker, N., Mertes, S., Weingartner, E. and Weinbruch, S.: Chemical
763 composition and mixing-state of ice residuals sampled within mixed phase clouds, Atmos.
764 Chem. Phys., 11, 2805–2816, doi:10.5194/acp-11-2805-2011, 2011.

765 Field, P. R., Heymsfield, A. J., Shipway, B. J., DeMott, P. J., Pratt, K. A., Rogers, D. C., Stith, J.
766 and Prather, K. A.: Ice in Clouds Experiment-Layer Clouds. Part II: Testing Characteristics of
767 Heterogeneous Ice Formation in Lee Wave Clouds, J. Atmos. Sci., 69, 1066–1079,
768 doi:10.1175/JAS-D-11-026.1, 2012.

769 Field, P. R., Möhler, O., Connolly, P., Krämer, M., Cotton, R., Heymsfield, A. J., Saathoff, H.
770 and Schnaiter, M.: Some ice nucleation characteristics of Asian and Saharan desert dust, Atmos.
771 Chem. Phys., 6, 2991–3006, doi:10.5194/acp-6-2991-2006, 2006.

772 Fletcher, N. H.: The Physics of Rainclouds, Cambridge University Press, Cambridge, United
773 Kingdom, 1962.

774 Friedman, B., Kulkarni, G., Beránek, J., Zelenyuk, A., Thornton, J. A. and Cziczo, D. J.: Ice
775 nucleation and droplet formation by bare and coated soot particles, J. Geophys. Res., 116,
776 D17203, doi:10.1029/2011JD015999, 2011.

777 Fröhlich-Nowoisky, J., Hill, T. C. J., Pummer, B. G., Yordanova, P., Franc, G. D. and Pöschl,
778 U.: Ice nucleation activity in the widespread soil fungus *Mortierella alpina*, Biogeosciences, 12,
779 1057–1071, doi:10.5194/bg-12-1057-2015, 2015.

780 Gabey, A. M., Gallagher, M. W., Whitehead, J., Dorsey, J. R., Kaye, P. H. and Stanley, W. R.:
781 Measurements and comparison of primary biological aerosol above and below a tropical forest
782 canopy using a dual channel fluorescence spectrometer, Atmos. Chem. Phys., 10, 4453–4466,
783 doi:10.5194/acp-10-4453-2010, 2010.

784 Gabey, A. M., Stanley, W. R., Gallagher, M. W. and Kaye, P. H.: The fluorescence properties of
785 aerosol larger than 0.8 μm in urban and tropical rainforest locations, Atmos. Chem. Phys., 11,
786 5491–5504, doi:10.5194/acp-11-5491-2011, 2011.

787 Gadi, R., Kulshrestha, U. C., Sarkar, A. K., Garg, S. C. and Parashar, D. C.: Emissions of SO_2
788 and NO_x from biofuels in India, Tellus B, 55, 787–795, doi:10.1034/j.1600-0889.2003.00065.x,
789 2003.

790 Galanter, M., Levy II, H. and Carmichael, G. R.: Impacts of biomass burning on tropospheric
791 CO, NO_x, and O_3, J. Geophys. Res., 105, 6633–6653, doi:10.1029/1999JD901113, 2000.

792 Garcia, E., Hill, T. C. J., Prenni, A. J., DeMott, P. J., Franc, G. D. and Kreidenweis, S. M.:
793 Biogenic ice nuclei in boundary layer air over two U.S. High Plains agricultural regions, J.
794 Geophys. Res., 117, D18209, doi:10.1029/2012JD018343, 2012.

795 Gaston, C. J., Pratt, K. A., Qin, X. and Prather, K. A.: Real-Time Detection and Mixing State of
796 Methanesulfonate in Single Particles at an Inland Urban Location during a Phytoplankton
797 Bloom, Environ. Sci. Technol., 44, 1566–1572, doi:10.1021/es902069d, 2010.

798 Gorbunov, B., Baklanov, A., Kakutkina, N., Windsor, H. L. and Toumi, R.: Ice nucleation on
799 soot particles, J. Aerosol Sci., 32, 199–215, doi:10.1016/s0021-8502(00)00077-x, 2001.

800 Hader, J. D., Wright, T. P. and Petters, M. D.: Contribution of pollen to atmospheric ice nuclei
801 concentrations, Atmos. Chem. Phys., 14, 5433–5449, doi:10.5194/acp-14-5433-2014, 2014.

802 Haga, D. I., Burrows, S. M., Iannone, R., Wheeler, M. J., Mason, R. H., Chen, J., Polishchuk, E.
803 A., Pöschl, U. and Bertram, A. K.: Ice nucleation by fungal spores from the classes
804 *Agaricomycetes*, *Ustilaginomycetes*, and *Eurotiomycetes*, and the effect on the atmospheric
805 transport of these spores, Atmos. Chem. Phys., 14, 8611–8630, doi:10.5194/acp-14-8611-2014,
806 2014.

807 Haga, D. I., Iannone, R., Wheeler, M. J., Mason, R., Polishchuk, E. A., Fetch Jr., T., van der
808 Kamp, B. J., McKendry, I. G. and Bertram, A. K.: Ice nucleation properties of rust and bunt
809 fungal spores and their transport to high altitudes, where they can cause heterogeneous freezing,
810 J. Geophys. Res.-Atmos., 118, 7260–7272, doi:10.1002/jgrd.50556, 2013.

811 Healy, D. A., Huffman, J. A., O'Connor, D. J., Pöhlker, C., Pöschl, U. and Sodeau, J. R.:
812 Ambient measurements of biological aerosol particles near Killarney, Ireland: a comparison
813 between real-time fluorescence and microscopy techniques, Atmos. Chem. Phys., 14, 8055–
814 8069, doi:10.5194/acp-14-8055-2014, 2014.

815 Healy, D. A., O'Connor, D. J., Burke, A. M. and Sodeau, J. R.: A laboratory assessment of the
816 Waveband Integrated Bioaerosol Sensor (WIBS-4) using individual samples of pollen and fungal
817 spore material, Atmos. Environ., 60, 534–543, doi:10.1016/j.atmosenv.2012.06.052, 2012a.

818 Healy, D. A., O'Connor, D. J. and Sodeau, J. R.: Measurement of the particle counting efficiency
819 of the "Waveband Integrated Bioaerosol Sensor" model number 4 (WIBS-4), J. Aerosol Sci., 47,
820 94–99, doi:10.1016/j.jaerosci.2012.01.003, 2012b.

821 Hill, T. C. J., Moffett, B. F., DeMott, P. J., Georgakopoulos, D. G., Stump, W. L. and Franc, G.
822 D.: Measurement of Ice Nucleation-Active Bacteria on Plants and in Precipitation by
823 Quantitative PCR, Appl. Environ. Microbiol., 80, 1256–1267, doi:10.1128/AEM.02967-13,
824 2014.

825 Hiranuma, N., Möhler, O., Yamashita, K., Tajiri, T., Saito, A., Kiselev, A., Hoffmann, N.,
826 Hoose, C., Jantsch, E., Koop, T. and Murakami, M.: Ice nucleation by cellulose and its potential
827 contribution to ice formation in clouds, Nat. Geosci., 8, 273–277, doi:10.1038/ngeo2374, 2015.

828 Hoose, C., Kristjánsson, J. E. and Burrows, S. M.: How important is biological ice nucleation in
829 clouds on a global scale?, Environ. Res. Lett., 5, 024009, doi:10.1088/1748-9326/5/2/024009,
830 2010a.

831 Hoose, C., Kristjánsson, J. E., Chen, J.-P. and Hazra, A.: A Classical-Theory-Based
832 Parameterization of Heterogeneous Ice Nucleation by Mineral Dust, Soot, and Biological
833 Particles in a Global Climate Model, J. Atmos. Sci., 67, 2483–2503,
834 doi:10.1175/2010JAS3425.1, 2010b.

835 Hoose, C. and Möhler, O.: Heterogeneous ice nucleation on atmospheric aerosols: a review of
836 results from laboratory experiments, Atmos. Chem. Phys., 12, 9817–9854, doi:10.5194/acp-12-
837 9817-2012, 2012.

838 Huffman, J. A., Prenni, A. J., DeMott, P. J., Pöhlker, C., Mason, R. H., Robinson, N. H.,
839 Fröhlich-Nowoisky, J., Tobo, Y., Després, V. R., Garcia, E., Gochis, D. J., Harris, E., Müller-
840 Germann, I., Ruzene, C., Schmer, B., Sinha, B., Day, D. A., Andreae, M. O., Jimenez, J. L.,
841 Gallagher, M., Kreidenweis, S. M., Bertram, A. K. and Pöschl, U.: High concentrations of
842 biological aerosol particles and ice nuclei during and after rain, Atmos. Chem. Phys., 13, 6151–
843 6164, doi:10.5194/acp-13-6151-2013, 2013.

844 Huffman, J. A., Sinha, B., Garland, R. M., Snee-Pollmann, A., Gunthe, S. S., Artaxo, P., Martin,
845 S. T., Andreae, M. O. and Pöschl, U.: Size distributions and temporal variations of biological
846 aerosol particles in the Amazon rainforest characterized by microscopy and real-time UV-APS
847 fluorescence techniques during AMAZE-08, Atmos. Chem. Phys., 12, 11997–12019,
848 doi:10.5194/acp-12-11997-2012, 2012.

849 Huffman, J. A., Treutlein, B. and Pöschl, U.: Fluorescent biological aerosol particle
850 concentrations and size distributions measured with an Ultraviolet Aerodynamic Particle Sizer
851 (UV-APS) in Central Europe, Atmos. Chem. Phys., 10, 3215–3233, doi:10.5194/acp-10-3215-
852 2010, 2010.

853 Iannone, R., Chernoff, D. I., Pringle, A., Martin, S. T. and Bertram, A. K.: The ice nucleation
854 ability of one of the most abundant types of fungal spores found in the atmosphere, Atmos.
855 Chem. Phys., 11, 1191–1201, doi:10.5194/acp-11-1191-2011, 2011.

856 Jayaweera, K. and Flanagan, P.: Investigations on biogenic ice nuclei in the Arctic atmosphere,
857 Geophys. Res. Lett., 9, 94–97, doi:10.1029/GL009i001p00094, 1982.

858 Jiang, H., Yin, Y., Su, H., Shan, Y. and Gao, R.: The characteristics of atmospheric ice nuclei
859 measured at the top of Huangshan (the Yellow Mountains) in Southeast China using a newly
860 built static vacuum water vapor diffusion chamber, Atmos. Res., 153, 200–208,
861 doi:10.1016/j.atmosres.2014.08.015, 2015.

862 Joly, M., Amato, P., Deguillaume, L., Monier, M., Hoose, C. and Delort, A.-M.: Quantification

of ice nuclei active at near 0 °C temperatures in low-altitude clouds at the Puy de Dôme atmospheric station, Atmos. Chem. Phys., 14, 8185–8195, doi:10.5194/acp-14-8185-2014, 2014.

Kamphus, M., Ettner-Mahl, M., Klimach, T., Drewnick, F., Keller, L., Cziczo, D. J., Mertes, S., Borrmann, S. and Curtius, J.: Chemical composition of ambient aerosol, ice residues and cloud droplet residues in mixed-phase clouds: single particle analysis during the Cloud and Aerosol Characterization Experiment (CLACE 6), Atmos. Chem. Phys., 10, 8077–8095, doi:10.5194/acp-10-8077-2010, 2010.

Kanji, Z. A. and Abbatt, J. P. D.: Ice Nucleation onto Arizona Test Dust at Cirrus Temperatures: Effect of Temperature and Aerosol Size on Onset Relative Humidity, J. Phys. Chem. A, 114, 935–941, doi:10.1021/jp908661m, 2010.

Kärcher, B., Möhler, O., DeMott, P. J., Pechtl, S. and Yu, F.: Insights into the role of soot aerosols in cirrus cloud formation, Atmos. Chem. Phys., 7, 4203–4227, doi:10.5194/acp-7-4203-2007, 2007.

Kaye, P., Stanley, W. R., Hirst, E., Foot, E. V, Baxter, K. L. and Barrington, S. J.: Single particle multichannel bio-aerosol fluorescence sensor, Opt. Express, 13, 3583–3593, doi:10.1364/OPEX.13.003583, 2005.

Keller, M. D.: Dimethyl Sulfide Production and Marine Phytoplankton: The Importance of Species Composition and Cell Size, Biol. Oceanogr., 6, 375–382, doi:10.1080/01965581.1988.10749540, 1989.

Kettle, A. J., Andreae, M. O., Amouroux, D., Andreae, T. W., Bates, T. S., Berresheim, H., Bingemer, H., Boniforti, R., Curran, M., DiTullio, G. R., Helas, G., Jones, G. B., Keller, M. D., Kiene, R. P., Leck, C., Levasseur, M., Malin, G., Maspero, M., Matrai, P., McTaggart, A. R., Mihalopoulos, N., Nguyen, B. C., Novo, A., Putaud, J. P., Rapsomanikis, S., Roberts, G., Schebeske, G., Sharma, S., Simó, R., Staubes, R., Turner, S. and Uher, G.: A global database of sea surface dimethylsulfide (DMS) measurements and a procedure to predict sea surface DMS as a function of latitude, longitude, and month, Glob. Biogeochem. Cy., 13, 399–444, doi:10.1029/1999GB900004, 1999.

Klein, H., Nickovic, S., Haunold, W., Bundke, U., Nillius, B., Ebert, M., Weinbruch, S., Schuetz, L., Levin, Z., Barrie, L. A. and Bingemer, H.: Saharan dust and ice nuclei over Central Europe, Atmos. Chem. Phys., 10, 10211–10221, doi:10.5194/acp-10-10211-2010, 2010.

Knopf, D. A., Alpert, P. A., Wang, B. and Aller, J. Y.: Stimulation of ice nucleation by marine diatoms, Nat. Geosci., 4, 88–90, doi:10.1038/ngeo1037, 2011.

Knopf, D. A., Alpert, P. A., Wang, B., O'Brien, R. E., Kelly, S. T., Laskin, A., Gilles, M. K. and Moffet, R. C.: Microspectroscopic imaging and characterization of individually identified ice nucleating particles from a case field study, J. Geophys. Res.-Atmos., 119, 10365–10381, doi:10.1002/2014JD021866, 2014.

Knopf, D. A. and Koop, T.: Heterogeneous nucleation of ice on surrogates of mineral dust, J. Geophys. Res., 111, D12201, doi:10.1029/2005JD006894, 2006.

Koop, T., Kapilashrami, A., Molina, L. T. and Molina, M. J.: Phase transitions of sea-salt/water mixtures at low temperatures: Implications for ozone chemistry in the polar marine boundary layer, J. Geophys. Res., 105, 26393–26402, doi:10.1029/2000JD900413, 2000.

Koop, T., Luo, B., Biermann, U. M., Crutzen, P. J. and Peter, T.: Freezing of $HNO_3/H_2SO_4/H_2O$ solutions at stratospheric temperatures: Nucleation statistics and experiments, J. Phys. Chem. A, 101, 1117–1133, doi:10.1021/jp9626531, 1997.

Kottek, M., Grieser, J., Beck, C., Rudolf, B. and Rubel, F.: World Map of the Köppen-Geiger climate classification updated, Meteorol. Z., 15, 259–263, doi:10.1127/0941-2948/2006/0130, 2006.

Kozloff, L. M., Schofield, M. A. and Lute, M.: Ice nucleating activity of Pseudomonas syringae and Erwinia herbicola, J. Bacteriol., 153, 222–231, 1983.

Kulkarni, G. and Dobbie, S.: Ice nucleation properties of mineral dust particles: determination of onset RH_i, IN active fraction, nucleation time-lag, and the effect of active sites on contact angles, Atmos. Chem. Phys., 10, 95–105, doi:10.5194/acp-10-95-2010, 2010.

Lee, H. J., Laskin, A., Laskin, J. and Nizkorodov, S. A.: Excitation-Emission Spectra and Fluorescence Quantum Yields for Fresh and Aged Biogenic Secondary Organic Aerosols, Environ. Sci. Technol., 47, 5763–5770, doi:10.1021/es400644c, 2013.

Leslie, J. F. and Summerell, B. A.: The *Fusarium* Laboratory Manual, Blackwell Publishing, Ames, Iowa, USA, 2006.

Lin, J. C., Matsui, T., Pielke Sr., R. A. and Kummerow, C.: Effects of biomass-burning-derived aerosols on precipitation and clouds in the Amazon Basin: a satellite-based empirical study, J. Geophys. Res., 111, D19204, doi:10.1029/2005JD006884, 2006.

Lindow, S. E., Arny, D. C. and Upper, C. D.: Erwinia herbicola: A Bacterial Ice Nucleus Active in Increasing Frost Injury to Corn, Phytopathology, 68, 523–527, 1978.

Liu, X., Penner, J. E. and Wang, M.: Influence of anthropogenic sulfate and black carbon on upper tropospheric clouds in the NCAR CAM3 model coupled to the IMPACT global aerosol model, J. Geophys. Res., 114, D03204, doi:10.1029/2008JD010492, 2009.

Lohmann, U.: A glaciation indirect aerosol effect caused by soot aerosols, Geophys. Res. Lett., 29, 1052, doi:10.1029/2001GL014357, 2002.

Lüönd, F., Stetzer, O., Welti, A. and Lohmann, U.: Experimental study on the ice nucleation ability of size-selected kaolinite particles in the immersion mode, J. Geophys. Res., 115, D14201, doi:10.1029/2009JD012959, 2010.

Maheshwari, R.: Fungi: Experimental Methods in Biology, CRC Press, Taylor & Francis Group, Boca Raton, Florida, USA, 2005.

Maki, L. R., Galyan, E. L., Chang-Chien, M.-M. and Caldwell, D. R.: Ice nucleation induced by pseudomonas syringae, Appl. Microbiol., 28, 456–459, 1974.

Maki, L. R. and Willoughby, K. J.: Bacteria as Biogenic Sources of Freezing Nuclei, J. Appl. Meteorol., 17, 1049–1053, 1978.

Marcolli, C., Gedamke, S., Peter, T. and Zobrist, B.: Efficiency of immersion mode ice nucleation on surrogates of mineral dust, Atmos. Chem. Phys., 7, 5081–5091, doi:10.5194/acp-7-5081-2007, 2007.

Maring, H., Savoie, D. L., Izaguirre, M. A., Custals, M. and Reid, J. S.: Mineral dust aerosol size distribution change during atmospheric transport, J. Geophys. Res., 108, 8592, doi:10.1029/2002JD002536, 2003.

Marple, V. A., Rubow, K. L. and Behm, S. M.: A Microorifice Uniform Deposit Impactor (MOUDI): Description, Calibration, and Use, Aerosol Sci. Technol., 14, 434–446, doi:10.1080/02786829108959504, 1991.

Mason, B. J. and Maybank, J.: Ice-nucleating properties of some natural mineral dusts, Q. J. R. Meteorol. Soc., 84, 235–241, doi:10.1002/qj.49708436104, 1958.

Mason, R. H., Chou, C., McCluskey, C. S., Levin, E. J. T., Schiller, C. L., Hill, T. C. J., Huffman, J. A., DeMott, P. J. and Bertram, A. K.: The micro-orifice uniform deposit impactor-droplet freezing technique (MOUDI-DFT) for measuring concentrations of ice nucleating particles as a function of size: improvements and initial validation, Atmos. Meas. Tech., 8, 2449–2462, doi:10.5194/amt-8-2449-2015, 2015.

McCluskey, C. S., DeMott, P. J., Prenni, A. J., Levin, E. J. T., McMeeking, G. R., Sullivan, A. P., Hill, T. C. J., Nakao, S., Carrico, C. M. and Kreidenweis, S. M.: Characteristics of atmospheric ice nucleating particles associated with biomass burning in the US: Prescribed burns and wildfires, J. Geophys. Res.-Atmos., 119, 10458–10470, doi:10.1002/2014JD021980, 2014.

McKendry, I. G., Christensen, E., Schiller, C. L., Vingarzan, R., Macdonald, A. M. and Li, Y.: Low Ozone Episodes at Amphitrite Point Marine Boundary Layer Observatory, British Columbia, Canada, Atmosphere-Ocean, 52, 271–280, doi:10.1080/07055900.2014.910164, 2014.

Meyers, M. P., DeMott, P. J. and Cotton, W. R.: New primary ice-nucleation parameterizations in an explicit cloud model, J. Appl. Meteorol., 31, 708–721, 1992.

Möhler, O., Büttner, S., Linke, C., Schnaiter, M., Saathoff, H., Stetzer, O., Wagner, R., Krämer, M., Mangold, A., Ebert, V. and Schurath, U.: Effect of sulfuric acid coating on heterogeneous ice nucleation by soot aerosol particles, J. Geophys. Res., 110, D11210, doi:10.1029/2004JD005169, 2005.

Möhler, O., DeMott, P. J., Vali, G. and Levin, Z.: Microbiology and atmospheric processes: the role of biological particles in cloud physics, Biogeosciences, 4, 1059–1071, doi:10.5194/bg-4-1059-2007, 2007.

Möhler, O., Field, P. R., Connolly, P., Benz, S., Saathoff, H., Schnaiter, M., Wagner, R., Cotton, R., Krämer, M., Mangold, A. and Heymsfield, A. J.: Efficiency of the deposition mode ice nucleation on mineral dust particles, Atmos. Chem. Phys., 6, 3007–3021, doi:10.5194/acp-6-3007-2006, 2006.

Monahan, E. C. and Muircheartaigh, I. Ó.: Optimal power-law description of oceanic whitecap coverage dependence on wind speed, J. Phys. Oceanogr., 10, 2094–2099, 1980.

Morris, C. E., Sands, D. C., Glaux, C., Samsatly, J., Asaad, S., Moukahel, A. R., Gonçalves, F. L. T. and Bigg, E. K.: Urediospores of rust fungi are ice nucleation active at > −10 °C and harbor ice nucleation active bacteria, Atmos. Chem. Phys., 13, 4223–4233, doi:10.5194/acp-13-4223-2013, 2013.

Morris, C. E., Sands, D. C., Vinatzer, B. A., Glaux, C., Guilbaud, C., Buffière, A., Yan, S., Dominguez, H. and Thompson, B. M.: The life history of the plant pathogen Pseudomonas syringae is linked to the water cycle, ISME J., 2, 321–334, doi:10.1038/ismej.2007.113, 2008.

Murray, B. J., Broadley, S. L., Wilson, T. W., Atkinson, J. D. and Wills, R. H.: Heterogeneous freezing of water droplets containing kaolinite particles, Atmos. Chem. Phys., 11, 4191–4207, doi:10.5194/acp-11-4191-2011, 2011.

Murray, B. J., O'Sullivan, D., Atkinson, J. D. and Webb, M. E.: Ice nucleation by particles immersed in supercooled cloud droplets, Chem. Soc. Rev., 41, 6519–6554, doi:10.1039/c2cs35200a, 2012.

National Data Buoy Center, National Oceanic and Atmospheric Administration, http://www.ndbc.noaa.gov/station_page.php?station=46206 (last accessed: 9 December 2014), 2013.

Niedermeier, D., Hartmann, S., Shaw, R. A., Covert, D., Mentel, T. F., Schneider, J., Poulain, L., Reitz, P., Spindler, C., Clauss, T., Kiselev, A., Hallbauer, E., Wex, H., Mildenberger, K. and Stratmann, F.: Heterogeneous freezing of droplets with immersed mineral dust particles - measurements and parameterization, Atmos. Chem. Phys., 10, 3601–3614, doi:10.5194/acp-10-3601-2010, 2010.

O'Dowd, C. D. and de Leeuw, G.: Marine aerosol production: a review of the current knowledge, Philos. Trans. R. Soc. A, 365, 1753–1774, doi:10.1098/rsta.2007.2043, 2007.

O'Sullivan, D., Murray, B. J., Malkin, T. L., Whale, T. F., Umo, N. S., Atkinson, J. D., Price, H. C., Baustian, K. J., Browse, J. and Webb, M. E.: Ice nucleation by fertile soil dusts: relative importance of mineral and biogenic components, Atmos. Chem. Phys., 14, 1853–1867, doi:10.5194/acp-14-1853-2014, 2014.

O'Sullivan, D., Murray, B. J., Ross, J. F., Whale, T. F., Price, H. C., Atkinson, J. D., Umo, N. S. and Webb, M. E.: The relevance of nanoscale biological fragments for ice nucleation in clouds, Sci. Rep., 5, 8082, doi:10.1038/srep08082, 2015.

Pan, Y.-L., Holler, S., Chang, R. K., Hill, S. C., Pinnick, R. G., Niles, S., Bottiger, J. R. and Bronk, B. V: Real-time detection and characterization of individual flowing airborne biological particles: fluorescence spectra and elastic scattering measurements, P. Soc. Photo-Opt. Ins., 3855, 117–125, doi:10.1117/12.371270, 1999.

Parker, L. V, Sullivan, C. W., Forest, T. W. and Ackley, S. F.: Ice nucleation activity of antarctic marine microorganisms, Antarct. J. US, 20, 126–127, 1985.

Penner, J. E., Chen, Y., Wang, M. and Liu, X.: Possible influence of anthropogenic aerosols on cirrus clouds and anthropogenic forcing, Atmos. Chem. Phys., 9, 879–896, doi:10.5194/acp-9-879-2009, 2009.

Petters, M. D., Parsons, M. T., Prenni, A. J., Demott, P. J., Kreidenweis, S. M., Carrico, C. M., Sullivan, A. P., McMeeking, G. R., Levin, E., Wold, C. E., Collett Jr., J. L. and Moosmüller, H.: Ice nuclei emissions from biomass burning, J. Geophys. Res., 114, D07209, doi:10.1029/2008JD011532, 2009.

Petzold, A., Kramer, H. and Schönlinner, M.: Continuous Measurement of Atmospheric Black Carbon Using a Multi-angle Absorption Photometer, Environ. Sci. Pollut. Res., 4, 78–82, 2002.

1023 Petzold, A., Ogren, J. A., Fiebig, M., Laj, P., Li, S.-M., Baltensperger, U., Holzer-Popp, T.,
1024 Kinne, S., Pappalardo, G., Sugimoto, N., Wehrli, C., Wiedensohler, A. and Zhang, X.-Y.:
1025 Recommendations for reporting "black carbon" measurements, Atmos. Chem. Phys., 13, 8365–
1026 8379, doi:10.5194/acp-13-8365-2013, 2013.

1027 Petzold, A., Schloesser, H., Sheridan, P. J., Arnott, W. P., Ogren, J. A. and Virkkula, A.:
1028 Evaluation of Multiangle Absorption Photometry for Measuring Aerosol Light Absorption,
1029 Aerosol Sci. Technol., 39, 40–51, doi:10.1080/027868290901945, 2005.

1030 Petzold, A. and Schönlinner, M.: Multi-angle absorption photometry - a new method for the
1031 measurement of aerosol light absorption and atmospheric black carbon, J. Aerosol Sci., 35, 421–
1032 441, doi:10.1016/j.jaerosci.2003.09.005, 2004.

1033 Phillips, V. T. J., Andronache, C., Christner, B., Morris, C. E., Sands, D. C., Bansemer, A.,
1034 Lauer, A., McNaughton, C. and Seman, C.: Potential impacts from biological aerosols on
1035 ensembles of continental clouds simulated numerically, Biogeosciences, 6, 987–1014,
1036 doi:10.5194/bg-6-987-2009, 2009.

1037 Phinney, L., Leaitch, W. R., Lohmann, U., Boudries, H., Worsnop, D. R., Jayne, J. T., Toom-
1038 Sauntry, D., Wadleigh, M., Sharma, S. and Shantz, N.: Characterization of the aerosol over the
1039 sub-arctic north east Pacific Ocean, Deep-Sea Res. Pt. II, 53, 2410–2433,
1040 doi:10.1016/j.dsr2.2006.05.044, 2006.

1041 Pöhlker, C., Huffman, J. A. and Pöschl, U.: Autofluorescence of atmospheric bioaerosols -
1042 fluorescent biomolecules and potential interferences, Atmos. Meas. Tech., 5, 37–71,
1043 doi:10.5194/amt-5-37-2012, 2012.

1044 Pouleur, S., Richard, C., Martin, J.-G. and Antoun, H.: Ice Nucleation Activity in *Fusarium*
1045 *acuminatum* and *Fusarium avenaceum*, Appl. Environ. Microbiol., 58, 2960–2964, 1992.

1046 Prather, K. A., Bertram, T. H., Grassian, V. H., Deane, G. B., Stokes, M. D., DeMott, P. J.,
1047 Aluwihare, L. I., Palenik, B. P., Azam, F., Seinfeld, J. H., Moffet, R. C., Molina, M. J., Cappa,
1048 C. D., Geiger, F. M., Roberts, G. C., Russell, L. M., Ault, A. P., Baltrusaitis, J., Collins, D. B.,
1049 Corrigan, C. E., Cuadra-Rodriguez, L. A., Ebben, C. J., Forestieri, S. D., Guasco, T. L., Hersey,
1050 S. P., Kim, M. J., Lambert, W. F., Modini, R. L., Mui, W., Pedler, B. E., Ruppel, M. J., Ryder,
1051 O. S., Schoepp, N. G., Sullivan, R. C. and Zhao, D.: Bringing the ocean into the laboratory to
1052 probe the chemical complexity of sea spray aerosol, P. Natl. Acad. Sci. USA, 110, 7550–7555,
1053 doi:10.1073/pnas.1300262110, 2013.

1054 Pratt, K. A., DeMott, P. J., French, J. R., Wang, Z., Westphal, D. L., Heymsfield, A. J., Twohy,
1055 C. H., Prenni, A. J. and Prather, K. A.: In situ detection of biological particles in cloud ice-
1056 crystals, Nat. Geosci., 2, 398–401, doi:10.1038/ngeo521, 2009.

1057 Prenni, A. J., Petters, M. D., Kreidenweis, S. M., Heald, C. L., Martin, S. T., Artaxo, P., Garland,
1058 R. M., Wollny, A. G. and Pöschl, U.: Relative roles of biogenic emissions and Saharan dust as
1059 ice nuclei in the Amazon basin, Nat. Geosci., 2, 402–405, doi:10.1038/ngeo517, 2009.

1060 Prenni, A. J., Tobo, Y., Garcia, E., DeMott, P. J., Huffman, J. A., McCluskey, C. S.,
1061 Kreidenweis, S. M., Prenni, J. E., Pöhlker, C. and Pöschl, U.: The impact of rain on ice nuclei
1062 populations at a forested site in Colorado, Geophys. Res. Lett., 40, 227–231,
1063 doi:10.1029/2012GL053953, 2013.

1064 Pummer, B. G., Bauer, H., Bernardi, J., Bleicher, S. and Grothe, H.: Suspendable
1065 macromolecules are responsible for ice nucleation activity of birch and conifer pollen, Atmos.
1066 Chem. Phys., 12, 2541–2550, doi:10.5194/acp-12-2541-2012, 2012.

1067 Ribalet, F., Marchetti, A., Hubbard, K. A., Brown, K., Durkin, C. A., Morales, R., Robert, M.,
1068 Swalwell, J. E., Tortell, P. D. and Armbrust, E. V.: Unveiling a phytoplankton hotspot at a
1069 narrow boundary between coastal and offshore waters, P. Natl. Acad. Sci. USA, 107, 16571–
1070 16576, doi:10.1073/pnas.1005638107, 2010.

1071 Richard, C., Martin, J.-G. and Pouleur, S.: Ice nucleation activity identified in some
1072 phytopathogenic *Fusarium* species, Phytoprotection, 77, 83–92, doi:10.7202/706104ar, 1996.

1073 Richardson, M. S., DeMott, P. J., Kreidenweis, S. M., Cziczo, D. J., Dunlea, E. J., Jimenez, J. L.,
1074 Thomson, D. S., Ashbaugh, L. L., Borys, R. D., Westphal, D. L., Casuccio, G. S. and Lersch, T.
1075 L.: Measurements of heterogeneous ice nuclei in the western United States in springtime and
1076 their relation to aerosol characteristics, J. Geophys. Res., 112, D02209,
1077 doi:10.1029/2006JD007500, 2007.

1078 Rogers, D. C., DeMott, P. J., Kreidenweis, S. M. and Chen, Y.: Measurements of ice nucleating
1079 aerosols during SUCCESS, Geophys. Res. Lett., 25, 1383–1386, doi:10.1029/97GL03478, 1998.

1080 Saltzman, E. S., Savoie, D. L., Prospero, J. M. and Zika, R. G.: Methanesulfonic acid and non-
1081 sea-salt sulfate in Pacific air: Regional and seasonal variations, J. Atmos. Chem., 4, 227–240,
1082 doi:10.1007/BF00052002, 1986.

1083 Savoie, D. L., Prospero, J. M., Arimoto, R. and Duce, R. A.: Non-sea-salt sulfate and
1084 methanesulfonate at American Samoa, J. Geophys. Res., 99, 3587–3596,
1085 doi:10.1029/93JD03337, 1994.

1086 Schnell, R. C.: Ice nuclei produced by laboratory cultured marine phytoplankton, Geophys. Res.
1087 Lett., 2, 500–502, doi:10.1029/GL002i011p00500, 1975.

1088 Schnell, R. C.: Ice Nuclei in Seawater, Fog Water and Marine Air off the Coast of Nova Scotia:
1089 Summer 1975, J. Atmos. Sci., 34, 1299–1305, 1977.

1090 Schnell, R. C. and Vali, G.: Freezing nuclei in marine waters, Tellus, 27, 321–323,
1091 doi:10.1111/j.2153-3490.1975.tb01682.x, 1975.

1092 Schroder, J. C., Hanna, S. J., Modini, R. L., Corrigan, A. L., Kreidenweis, S. M., Macdonald, A.
1093 M., Noone, K. J., Russell, L. M., Leaitch, W. R. and Bertram, A. K.: Size-resolved observations
1094 of refractory black carbon particles in cloud droplets at a marine boundary layer site, Atmos.
1095 Chem. Phys., 15, 1367–1383, doi:10.5194/acp-15-1367-2015, 2015.

1096 Schwarz, J. P., Gao, R. S., Perring, A. E., Spackman, J. R. and Fahey, D. W.: Black carbon
1097 aerosol size in snow, Sci. Rep., 3, 1356, doi:10.1038/srep01356, 2013.

1098 Schwarz, J. P., Gao, R. S., Spackman, J. R., Watts, L. A., Thomson, D. S., Fahey, D. W.,
1099 Ryerson, T. B., Peischl, J., Holloway, J. S., Trainer, M., Frost, G. J., Baynard, T., Lack, D. A., de
1100 Gouw, J. A., Warneke, C. and Del Negro, L. A.: Measurement of the mixing state, mass, and
1101 optical size of individual black carbon particles in urban and biomass burning emissions,
1102 Geophys. Res. Lett., 35, L13810, doi:10.1029/2008GL033968, 2008.

1103 Sesartic, A., Lohmann, U. and Storelvmo, T.: Modelling the impact of fungal spore ice nuclei on
1104 clouds and precipitation, Environ. Res. Lett., 8, 014029, doi:10.1088/1748-9326/8/1/014029,
1105 2013.

1106 Sivaprakasam, V., Huston, A., Scotto, C. and Eversole, J.: Multiple UV wavelength excitation
1107 and fluorescence of bioaerosols, Opt. Express, 12, 4457–4466, doi:10.1364/OPEX.12.004457,
1108 2004.

1109 Sorooshian, A., Padró, L. T., Nenes, A., Feingold, G., McComiskey, A., Hersey, S. P., Gates, H.,
1110 Jonsson, H. H., Miller, S. D., Stephens, G. L., Flagan, R. C. and Seinfeld, J. H.: On the link
1111 between ocean biota emissions, aerosol, and maritime clouds: Airborne, ground, and satellite
1112 measurements off the coast of California, Global Biogeochem. Cycles, 23, GB4007,
1113 doi:10.1029/2009GB003464, 2009.

1114 Spracklen, D. V and Heald, C. L.: The contribution of fungal spores and bacteria to regional and
1115 global aerosol number and ice nucleation immersion freezing rates, Atmos. Chem. Phys., 14,
1116 9051–9059, doi:10.5194/acp-14-9051-2014, 2014.

1117 Statistics Canada, Catalogue no. 98-316-XWE, available at: http://www12.statcan.gc.ca/census-
1118 recensement/2011/dp-pd/prof/index.cfm?Lang=E (last access: 4 November 2014), Ottawa, 2012.

1119 Storelvmo, T., Hoose, C. and Eriksson, P.: Global modeling of mixed-phase clouds: The albedo
1120 and lifetime effects of aerosols, J. Geophys. Res., 116, D05207, doi:10.1029/2010JD014724,
1121 2011.

1122 Sun, J., Ariya, P. A., Leighton, H. G. and Yau, M. K.: Modeling Study of Ice Formation in
1123 Warm-Based Precipitating Shallow Cumulus Clouds, J. Atmos. Sci., 69, 3315–3335,
1124 doi:10.1175/JAS-D-11-0344.1, 2012.

1125 Szyrmer, W. and Zawadzki, I.: Biogenic and anthropogenic sources of ice-forming nuclei: A
1126 review, B. Am. Meteorol. Soc., 78, 209–228, 1997.

1127 Tobo, Y., DeMott, P. J., Hill, T. C. J., Prenni, A. J., Swoboda-Colberg, N. G., Franc, G. D. and
1128 Kreidenweis, S. M.: Organic matter matters for ice nuclei of agricultural soil origin, Atmos.
1129 Chem. Phys., 14, 8521–8531, doi:10.5194/acp-14-8521-2014, 2014.

1130 Tobo, Y., Prenni, A. J., DeMott, P. J., Huffman, J. A., McCluskey, C. S., Tian, G., Pöhlker, C.,
1131 Pöschl, U. and Kreidenweis, S. M.: Biological aerosol particles as a key determinant of ice nuclei
1132 populations in a forest ecosystem, J. Geophys. Res.-Atmos., 118, 10100–10110,
1133 doi:10.1002/jgrd.50801, 2013.

1134 Tsumuki, H., Konno, H., Maeda, T. and Okamoto, Y.: An ice-nucleating active fungus isolated
1135 from the gut of the rice stem borer, *Chilo suppressalis* Walker (Lepidoptera: Pyralidae), J. Insect
1136 Physiol., 38, 119–125, doi:10.1016/0022-1910(92)90040-K, 1992.

1137 Twohy, C. H., DeMott, P. J., Pratt, K. A., Subramanian, R., Kok, G. L., Murphy, S. M., Lersch,
1138 T., Heymsfield, A. J., Wang, Z., Prather, K. A. and Seinfeld, J. H.: Relationships of Biomass-
1139 Burning Aerosols to Ice in Orographic Wave Clouds, J. Atmos. Sci., 67, 2437–2450,
1140 doi:10.1175/2010JAS3310.1, 2010.

1141 United States Environmental Protection Agency, Air Emission Sources,
1142 http://www.epa.gov/air/emissions/index.htm (last access: 7 April 2015), 2014.

1143 Vali, G.: Quantitative Evaluation of Experimental Results on the Heterogeneous Freezing
1144 Nucleation of Supercooled Liquids, J. Atmos. Sci., 28, 402–409, 1971.

1145 Vali, G.: Nucleation Terminology, J. Aerosol Sci., 16, 575–576, doi:10.1016/0021-
1146 8502(85)90009-6, 1985.

1147 Vali, G., DeMott, P. J., Möhler, O. and Whale, T. F.: Technical Note: A proposal for ice
1148 nucleation terminology, Atmos. Chem. Phys., 15, 10263–10270, doi:10.5194/acp-15-10263-
1149 2015, 2015.

1150 von Blohn, N., Mitra, S. K., Diehl, K. and Borrmann, S.: The ice nucleating ability of pollen:
1151 Part III. New laboratory studies in immersion and contact freezing modes including more pollen
1152 types, Atmos. Res., 78, 182–189, doi:10.1016/j.atmosres.2005.03.008, 2005.

1153 Webster, J. and Weber, R. W. S.: Introduction to Fungi, Third Edition, Cambridge University
1154 Press, New York, NY, USA, 2007.

1155 Welti, A., Lüönd, F., Kanji, Z. A., Stetzer, O. and Lohmann, U.: Time dependence of immersion
1156 freezing: an experimental study on size selected kaolinite particles, Atmos. Chem. Phys., 12,
1157 9893–9907, doi:10.5194/acp-12-9893-2012, 2012.

1158 Wheeler, M. J. and Bertram, A. K.: Deposition nucleation on mineral dust particles: a case
1159 against classical nucleation theory with the assumption of a single contact angle, Atmos. Chem.
1160 Phys., 12, 1189–1201, doi:10.5194/acp-12-1189-2012, 2012.

1161 Wheeler, M. J., Mason, R. H., Steunenberg, K., Wagstaff, M., Chou, C. and Bertram, A. K.:
1162 Immersion Freezing of Supermicron Mineral Dust Particles: Freezing Results, Testing Different
1163 Schemes for Describing Ice Nucleation, and Ice Nucleation Active Site Densities, J. Phys. Chem.
1164 A, 119, 4358–4372, doi:10.1021/jp507875q, 2015.

1165 Whitney, F. A., Crawford, W. R. and Harrison, P. J.: Physical processes that enhance nutrient
1166 transport and primary productivity in the coastal and open ocean of the subarctic NE Pacific,
1167 Deep Sea Res. Part II Top. Stud. Oceanogr., 52, 681–706, doi:10.1016/j.dsr2.2004.12.023, 2005.

1168 Wilson, T. W., Ladino, L. A., Alpert, P. A., Breckels, M. N., Brooks, I. M., Browse, J., Burrows,
1169 S. M., Carslaw, K. S., Huffman, J. A., Judd, C., Kilthau, W. P., Mason, R. H., McFiggans, G.,
1170 Miller, L. A., Nájera, J. J., Polishchuk, E., Rae, S., Schiller, C. L., Si, M., Vergara Temprado, J.,
1171 Whale, T. F., Wong, J. P. S., Wurl, O., Yakobi-Hancock, J. D., Abbatt, J. P. D., Aller, J. Y.,
1172 Bertram, A. K., Knopf, D. A. and Murray, B. J.: A marine biogenic source of atmospheric ice
1173 nucleating particles, Nature, 525, 234–238, doi:10.1038/nature14986, 2015.

1174 Wright, T. P. and Petters, M. D.: The role of time in heterogeneous freezing nucleation, J.
1175 Geophys. Res.-Atmos., 118, 3731–3743, doi:10.1002/jgrd.50365, 2013.

1176 Wright, T. P., Petters, M. D., Hader, J. D., Morton, T. and Holder, A. L.: Minimal cooling rate
1177 dependence of ice nuclei activity in the immersion mode, J. Geophys. Res.-Atmos., 118, 10535–
1178 10543, doi:10.1002/jgrd.50810, 2013.

1179 Yakobi-Hancock, J. D., Ladino, L. A. and Abbatt, J. P. D.: Feldspar minerals as efficient
1180 deposition ice nuclei, Atmos. Chem. Phys., 13, 11175–11185, doi:10.5194/acp-13-11175-2013,
1181 2013.

1182 Yakobi-Hancock, J. D., Ladino, L. A., Bertram, A. K., Huffman, J. A., Jones, K., Leaitch, W. R.,
1183 Mason, R. H., Schiller, C. L., Toom-Sauntry, D., Wong, J. P. S. and Abbatt, J. P. D.: CCN

activity of size-selected aerosol at a Pacific coastal location, Atmos. Chem. Phys., 14, 12307–12317, doi:10.5194/acp-14-12307-2014, 2014.

Yang, M., Howell, S. G., Zhuang, J. and Huebert, B. J.: Attribution of aerosol light absorption to black carbon, brown carbon, and dust in China - interpretations of atmospheric measurements during EAST-AIRE, Atmos. Chem. Phys., 9, 2035–2050, doi:10.5194/acp-9-2035-2009, 2009.

Yun, Y. and Penner, J. E.: An evaluation of the potential radiative forcing and climatic impact of marine organic aerosols as heterogeneous ice nuclei, Geophys. Res. Lett., 40, 4121–4126, doi:10.1002/grl.50794, 2013.

Zimmermann, F., Weinbruch, S., Schütz, L., Hofmann, H., Ebert, M., Kandler, K. and Worringen, A.: Ice nucleation properties of the most abundant mineral dust phases, J. Geophys. Res., 113, D23204, doi:10.1029/2008JD010655, 2008.

Table 1. Correlation coefficients (R) for linear regression analyses of INPs versus fluorescent bioparticles, total aerosol particles, eBC, sodium, MSA, and wind speed[a]. Correlations with statistical significance ($P < 0.05$) are shown in bold.

	Relation to the INP number concentration											
	-15 °C			-20 °C			-25 °C			-30 °C		
Measurement	R	P[b]	n[c]	R	P	n	R	P	n	R	P	n
Fluorescent bioparticles [0.5–10 µm]	**0.74**	< 0.01	28	**0.77**	< 0.01	28	**0.83**	< 0.01	28	**0.66**	< 0.01	23
Total particles [0.5–10 µm]	**0.33**	0.04	28	**0.36**	0.03	28	**0.49**	< 0.01	28	**0.66**	< 0.01	23
eBC	**0.47**	< 0.01	34	**0.59**	< 0.01	34	**0.60**	< 0.01	34	0.25	0.11	27
Sodium	-0.35	0.25	6	0.13	0.40	6	0.32	0.27	6	0.82	0.20	3
MSA	0.17	0.38	6	0.51	0.15	6	0.27	0.30	6	0.00	0.50	3
(Wind speed)$^{3.41}$ [lighthouse]	0.05	0.39	34	0.01	0.48	34	0.15	0.19	34	**0.48**	< 0.01	27
(Wind speed)$^{3.41}$ [buoy]	0.04	0.40	34	0.04	0.40	34	0.19	0.14	34	**0.55**	< 0.01	27

[a]Using the power law dependence of whitecap coverage on wind speed found by Monahan and Muircheartaigh (1980), wind speed was raised to the power of 3.41.
[b]The P value is a conditional probability that is the probability of obtaining an R value equal to or greater than the given R value if there is no correlation between INPs and the given parameter.
[c]n represents the number of data points used in determining the correlation.

Table 2. Correlation coefficients (R) for linear regression analyses of INPs versus fluorescent bioparticles, total aerosol particles, eBC, and wind speed[a] within each category of air mass. Correlations with statistical significance ($P < 0.05$) are shown in bold.

		Relation to the INP number concentration											
		-15 °C			-20 °C			-25 °C			-30 °C		
Air Mass	Measurement	*R*	*P*[b]	*n*[c]	*R*	*P*	*n*	*R*	*P*	*n*	*R*	*P*	*n*
Coastal NW	Fluorescent bioparticles [0.5–10 µm]	**0.94**	<0.01	9	**0.94**	<0.01	9	**0.96**	<0.01	9	0.65	0.08	6
	Total particles [0.5–10 µm]	**0.85**	<0.01	9	**0.70**	0.02	9	**0.71**	0.02	9	0.67	0.07	6
	eBC	**0.71**	<0.01	11	**0.80**	<0.01	11	**0.84**	<0.01	11	0.53	0.11	7
	(Wind speed)$^{3.41}$ [lighthouse]	-0.38	0.12	11	-0.39	0.12	11	-0.22	0.26	11	0.26	0.29	7
	(Wind speed)$^{3.41}$ [buoy]	-0.03	0.47	11	0.00	0.49	11	0.00	0.50	11	-0.02	0.48	7
Coastal SE	Fluorescent bioparticles [0.5–10 µm]	-0.07	0.48	3	-0.53	0.32	3	-0.85	0.17	3	NA[d]		
	Total particles [0.5–10 µm]	-0.17	0.45	3	-0.61	0.29	3	-0.90	0.14	3	NA		
	eBC	0.07	0.46	5	0.28	0.32	5	0.67	0.11	5	0.96	0.09	3
	(Wind speed)$^{3.41}$ [lighthouse]	-0.34	0.29	5	-0.27	0.33	5	-0.14	0.41	5	0.21	0.43	3
	(Wind speed)$^{3.41}$ [buoy]	-0.52	0.18	5	-0.37	0.27	5	-0.12	0.43	5	0.93	0.12	3
Pacific Ocean	Fluorescent bioparticles [0.5–10 µm]	**0.80**	<0.01	12	**0.74**	<0.01	12	**0.64**	0.01	12	0.23	0.24	12
	Total particles [0.5–10 µm]	0.13	0.34	12	0.30	0.17	12	0.21	0.25	12	0.25	0.22	12
	eBC	0.24	0.21	14	0.37	0.10	14	0.26	0.19	14	0.06	0.42	13
	(Wind speed)$^{3.41}$ [lighthouse]	-0.10	0.37	14	-0.26	0.18	14	-0.26	0.19	14	-0.21	0.25	13
	(Wind speed)$^{3.41}$ [buoy]	-0.18	0.27	14	-0.38	0.09	14	**-0.48**	0.04	14	-0.22	0.23	13
Free troposphere	Fluorescent bioparticles [0.5–10 µm]	**0.97**	0.02	4	**0.99**	<0.01	4	**0.99**	<0.01	4	**1.00**	<0.01	4
	Total particles [0.5–10 µm]	0.86	0.07	4	**0.98**	0.01	4	**0.99**	<0.01	4	**0.98**	0.01	4
	eBC	**0.99**	<0.01	4	0.89	0.05	4	0.88	0.06	4	0.89	0.06	4
	(Wind speed)$^{3.41}$ [lighthouse]	-0.89	0.05	4	-0.70	0.15	4	-0.67	0.17	4	-0.68	0.16	4
	(Wind speed)$^{3.41}$ [buoy]	0.62	0.19	4	0.39	0.31	4	0.38	0.31	4	0.42	0.29	4

[a]Using the power law dependence of whitecap coverage on wind speed found by Monahan and Muircheartaigh (1980), wind speed was raised to the power of 3.41.
[b]The P value is a conditional probability that is the probability of obtaining an R value equal to or greater than the given R value if there is no correlation between INPs and the given parameter.
[c]n represents the number of data points used in determining the correlation.
[d]NA = not available due to insufficient data.

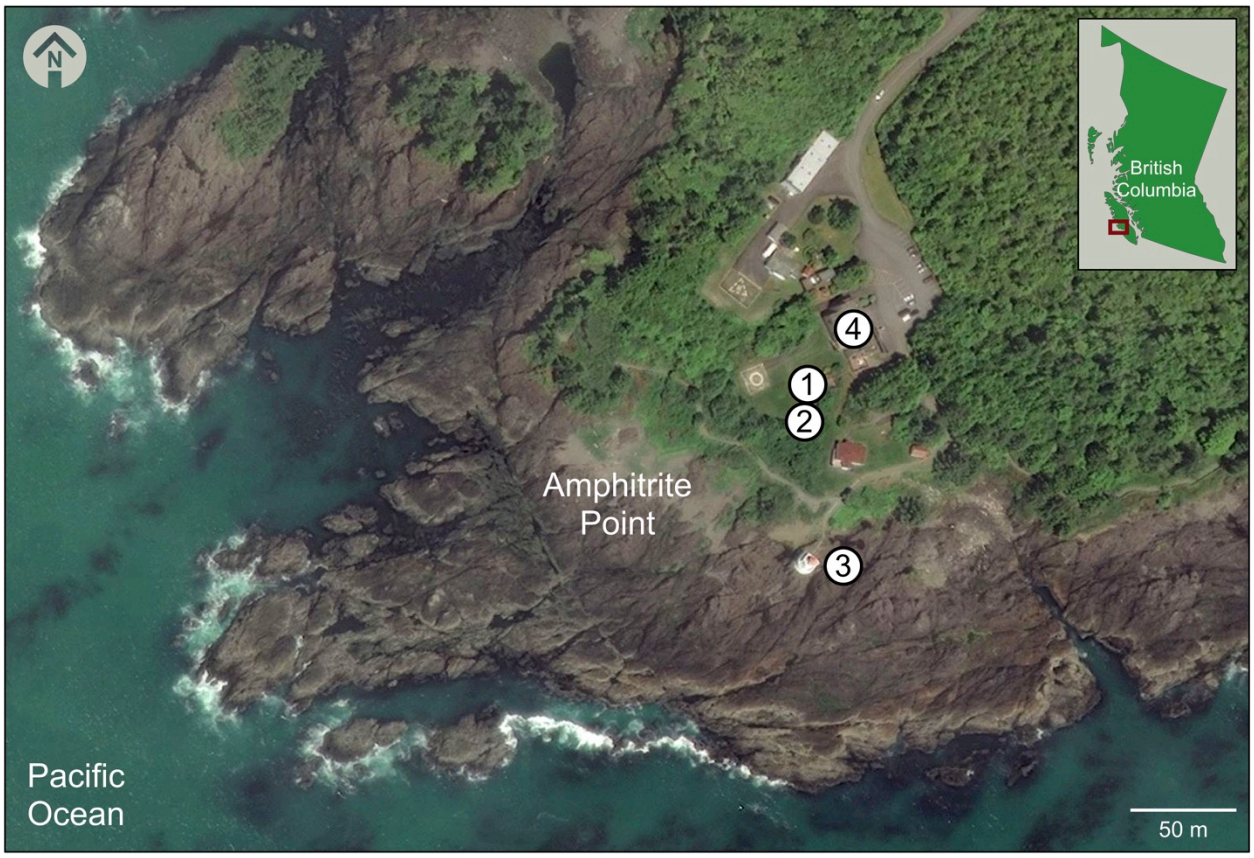

Figure 1. A satellite image of the sampling site: (1) location of the MOUDIs and the WIBS-4A; (2) location of the MAAP; (3) Amphitrite Lighthouse where most meteorological data was collected; and (4) a station of the Canadian Coast Guard with supporting infrastructure. The image was modified from Bing Maps, 2014 (http://www.bing.com/maps/). Inset: the location of the sampling site in British Columbia, Canada.

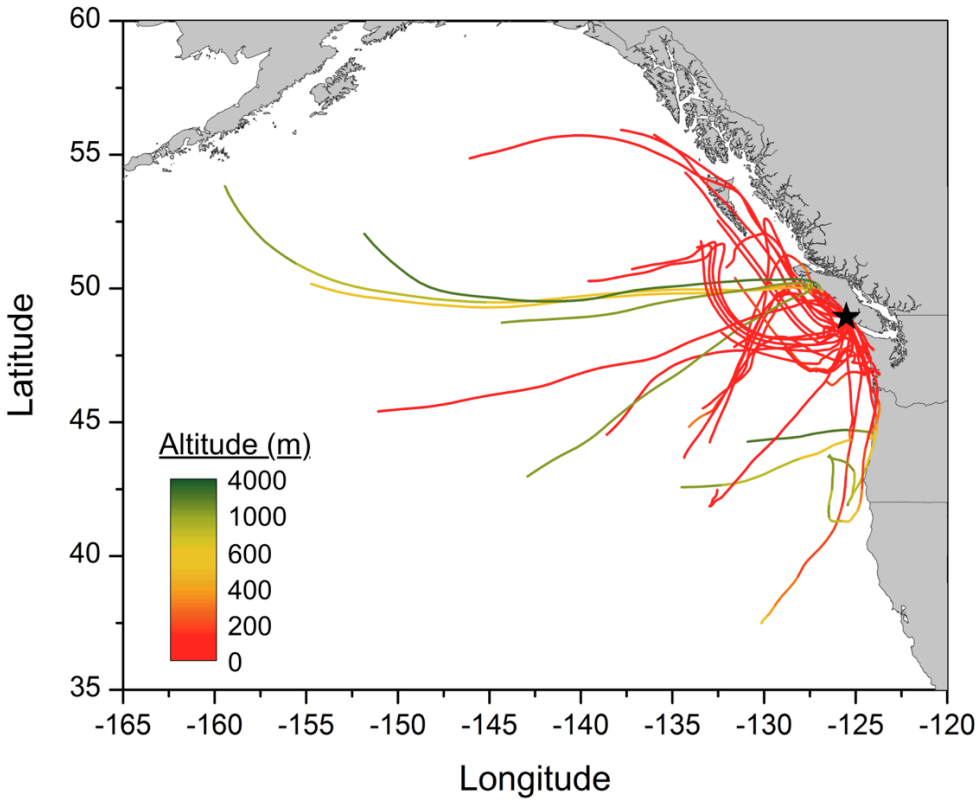

Figure 2. Seventy-two hour HYSPLIT4 back trajectories of the air masses analyzed at the coastal site (black star) during INP sampling periods. Each back trajectory was initiated from a height of 5.5 m agl and at the midpoint of the sampling period.

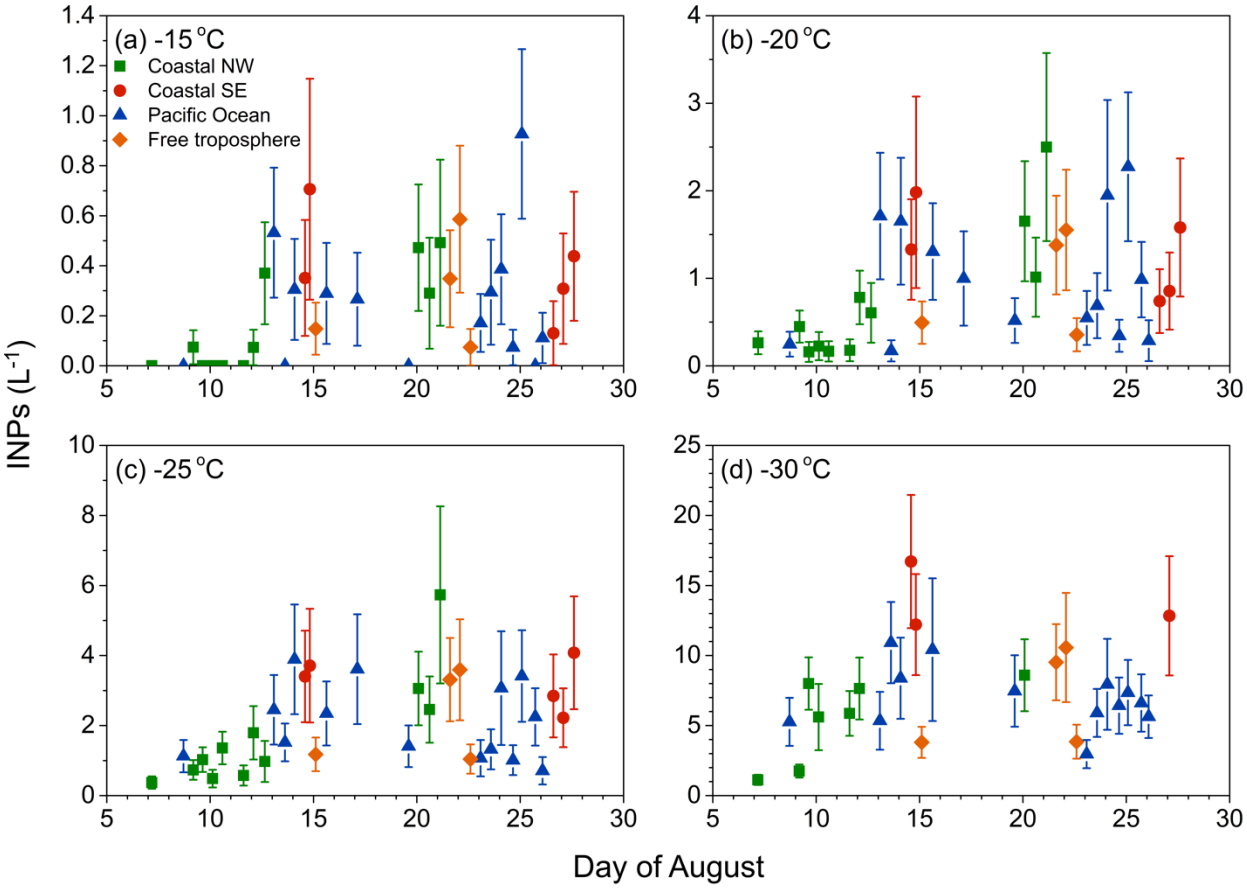

Figure 3. INP number concentrations as a function of date determined at ice-activation temperatures of (a) -15 °C, (b) -20 °C, (c) -25 °C, and (d) -30 °C. The symbols are color coded by air mass category (see Sect. 2.8 for details). Fewer data points are available at -30 °C as INP number concentrations can only be determined to the temperature where all droplets are frozen and Eq. (1) becomes undefined.

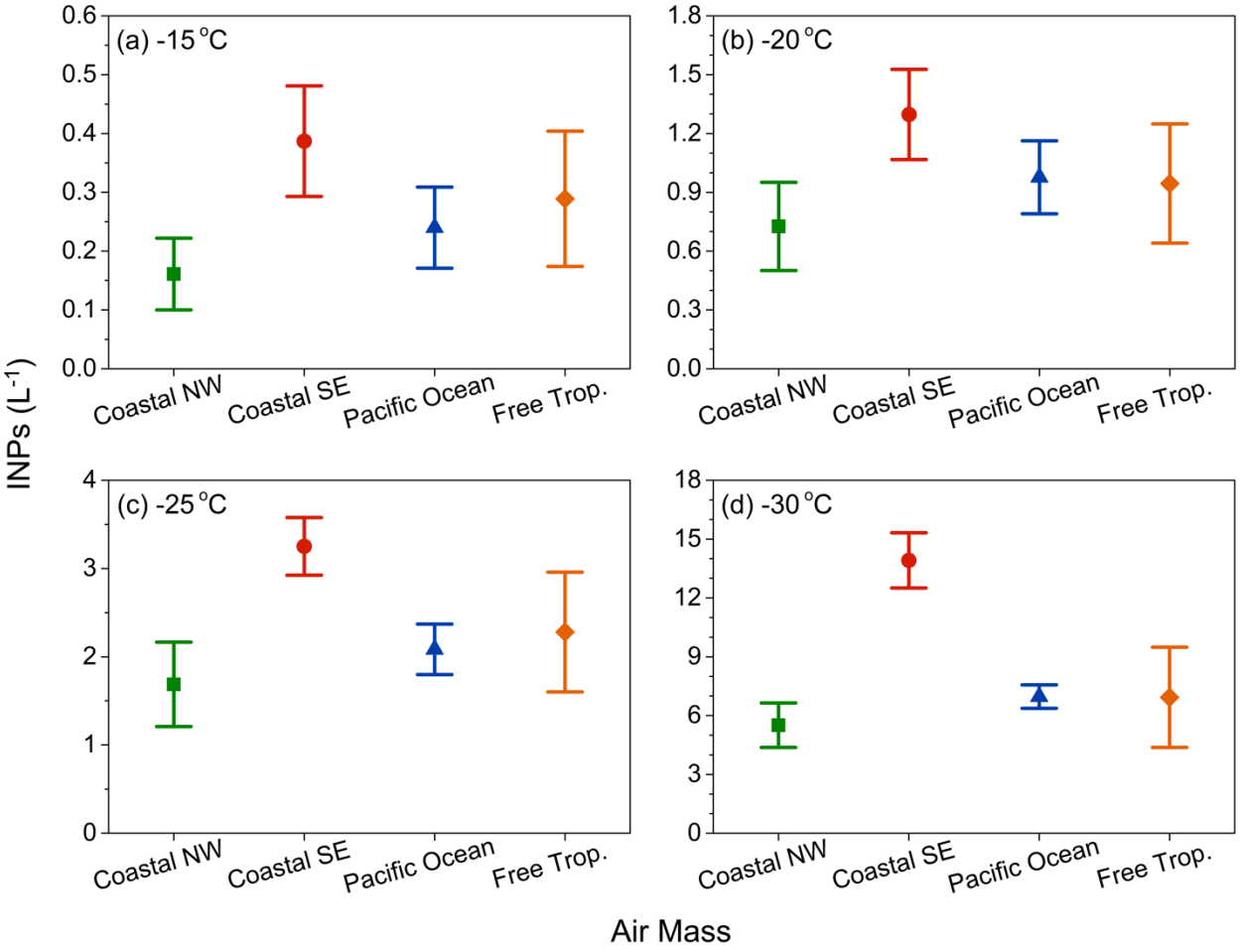

Figure 4. Mean INP number concentrations found in each of the four categories of air masses sampled at (a) -15 °C, (b) -20 °C, (c) -25 °C, and (d) -30 °C. The scheme for air mass classification is given in Sect. 2.8. Uncertainties are given as the standard error of the mean.

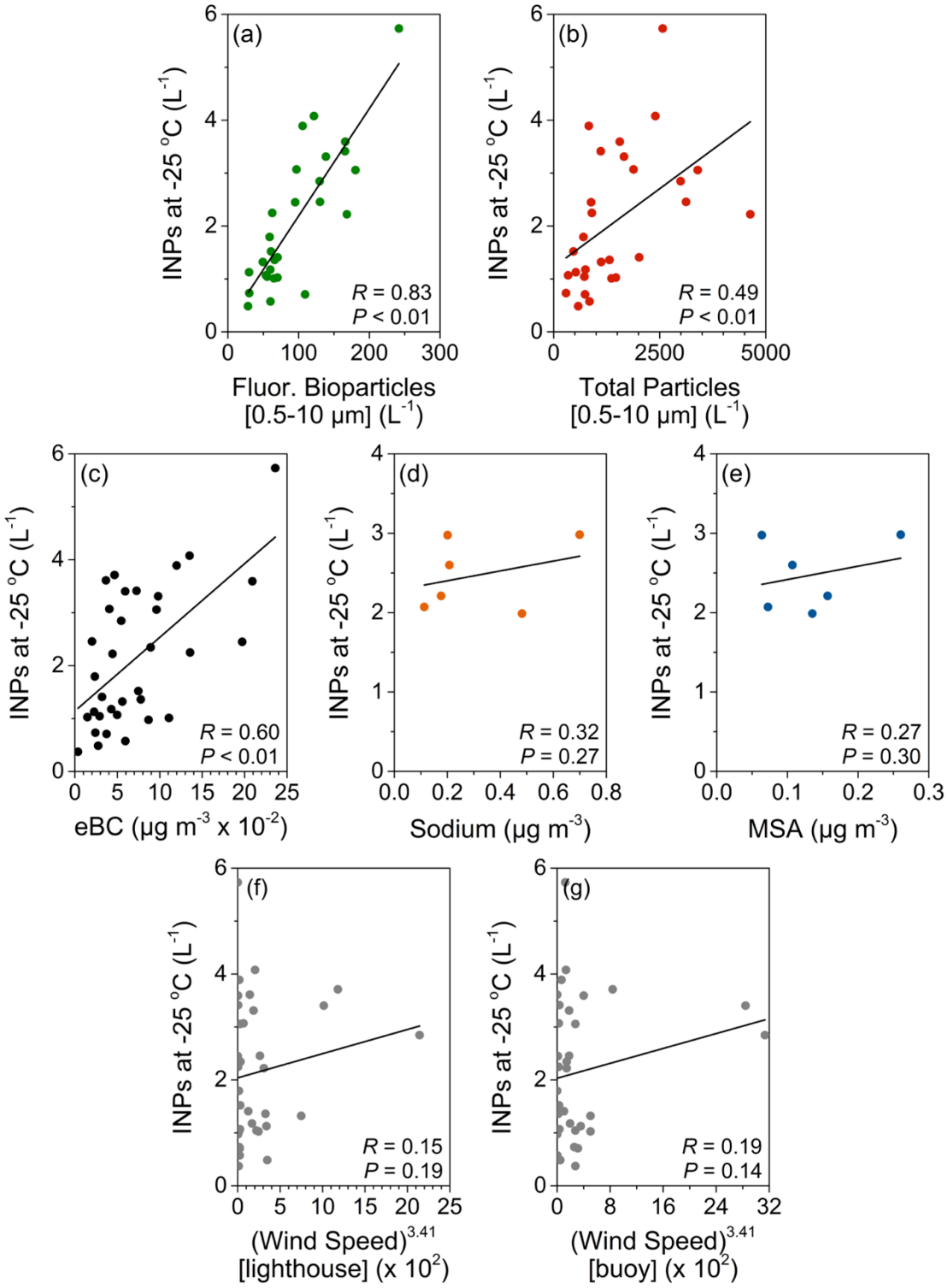

Figure 5. Number concentrations of INPs active at -25 °C plotted against concentrations of (a) fluorescent bioparticles 0.5–10 µm, (b) total particles 0.5–10 µm, (c) eBC, (d) sodium, (e) MSA, and (f–g) (wind speed)$^{3.41}$ based on the power law function of Monahan and Muircheartaigh (1980) where wind speed was in units of m s^{-1}. Linear fits are shown with corresponding correlation coefficients (R) and probability values (P).

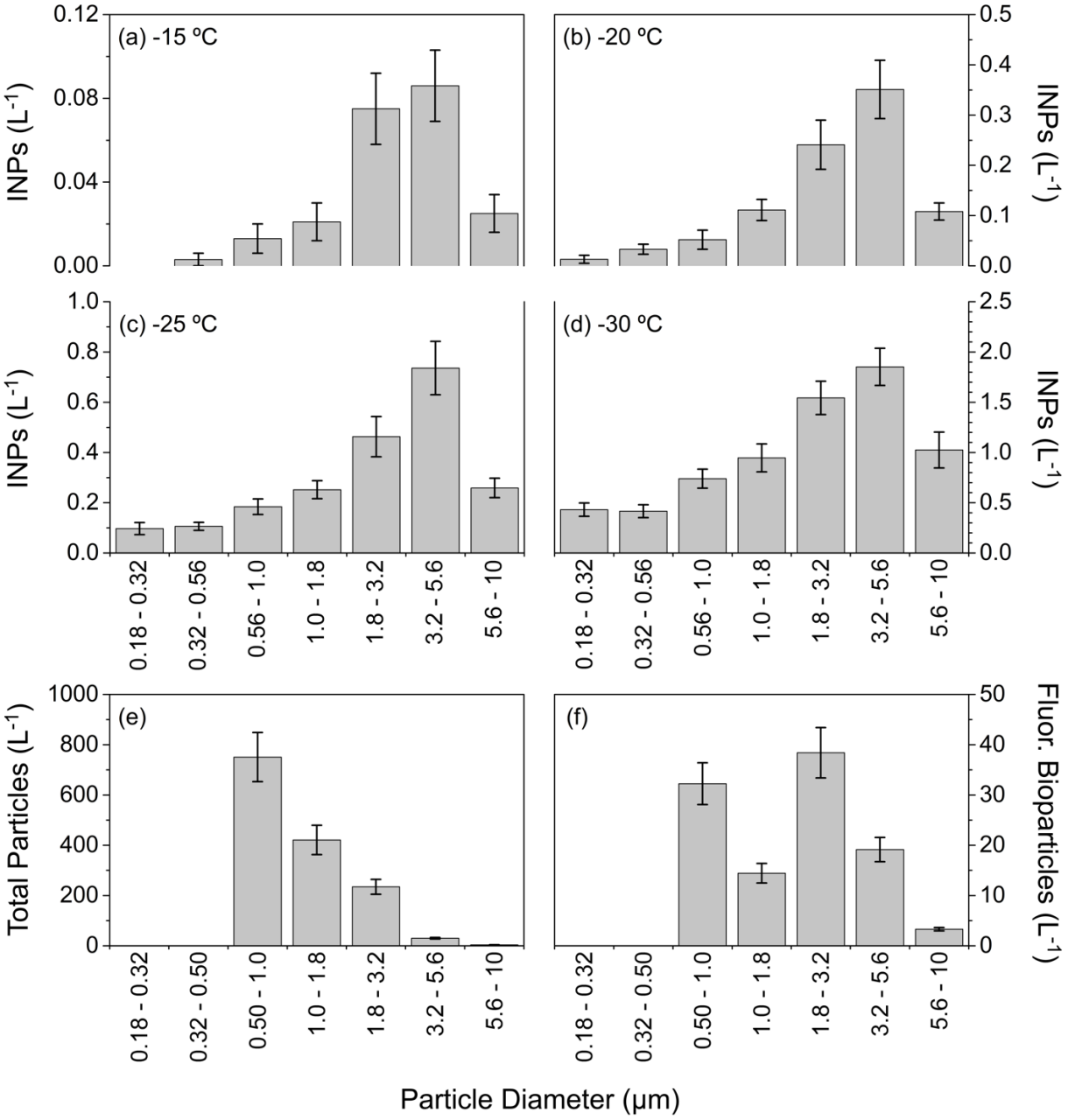

Figure 6. Mean number concentrations as a function of size for INPs active at (a) -15 °C, (b) -20 °C, (c) -25 °C, and (d) -30 °C, and total particles between 0.5 and 10 µm (e) and fluorescent bioparticles between 0.5 and 10 µm (f). Here we use only samples where both the MOUDI-DFT and WIBS-4A were operating. Uncertainties are given as the standard error of the mean. As INP number concentrations can only be determined at temperatures less than the temperature where all droplets are frozen and Eq. (1) becomes undefined, fewer samples are represented at -30 °C. Number concentrations below 0.5 µm were not measured by the WIBS-4A for panels (e) and (f) but plot axes are consistent for easier comparison of the size distributions.

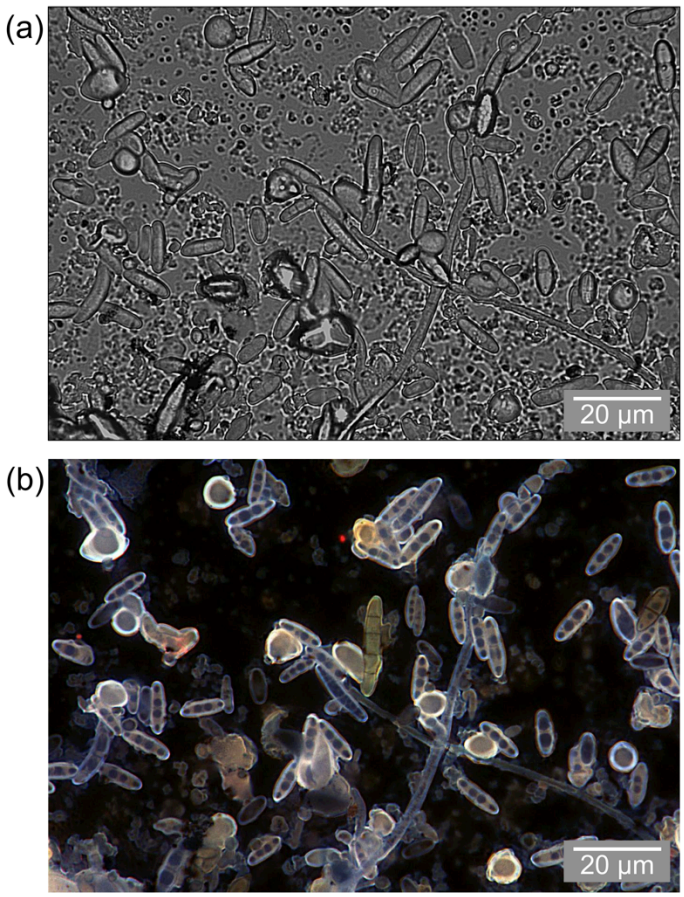

Figure 7. Fluorescence microscopy images of an aerosol sample collected on August 11, 2013: (a) bright-field image; (b) an overlay of red, green, and blue fluorescence channels. A blue coloration is characteristic of biological material (Pöhlker et al., 2012).

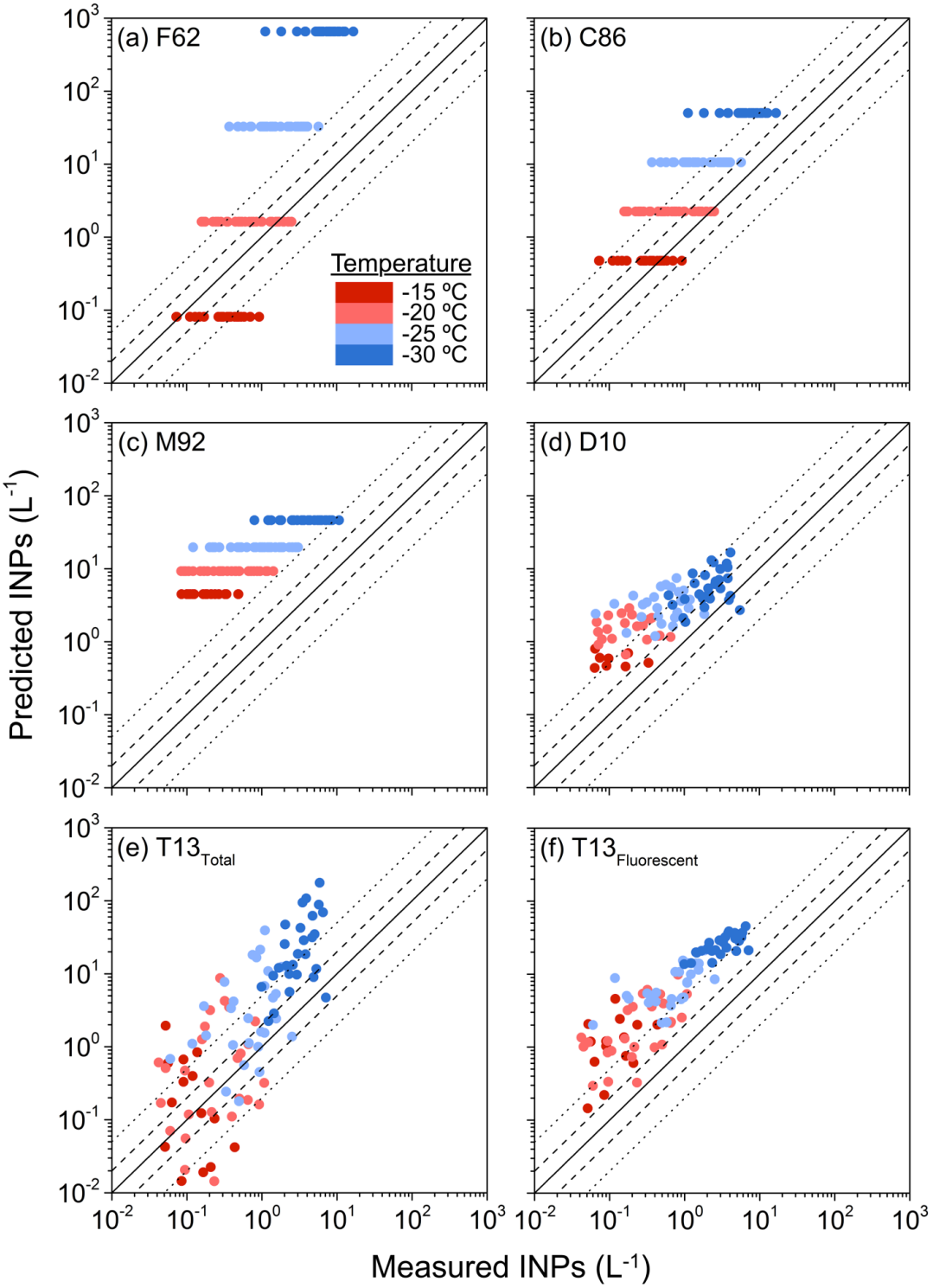

Figure 8. Predicted versus measured INP number concentrations based on the parameterizations of (a) Fletcher (1962); (b) Cooper (1986); (c) Meyers et al. (1992); (d) DeMott et al. (2010); and (e–f) Tobo et al. (2013). Details on these parameterizations are given in the Supplement. Data color represents ice nucleation temperatures. This figure uses the format of Fig. 9 in Tobo et al. (2013).